AD-766 444

# MODELING OF THE HUMAN FORCE AND MOTION-SENSING MECHANISMS

AIR FORCE HUMAN RESOURCES LABORATORY

JUNE 1973

AFHRL-TR-72-54



# MODELING OF THE HUMAN FORCE AND MOTION-SENSING MECHANISMS

*DON R. GUM*



TECHNICAL REPORT AFHRL-TR-72-54

JUNE 1973



Approved for public release; distribution unlimited.

ADVANCED SYSTEMS DIVISION
AIR FORCE HUMAN RESOURCES LABORATORY
AIR FORCE SYSTEMS COMMAND
WRIGHT-PATTERSON AIR FORCE BASE, OHIO

NOTICE

When Government drawings, specifications, or other data are used for any purpose other than in connection with a definitely related Government procurement operation, the United States Government thereby incurs no responsibility nor any obligation whatsoever; and the fact that the government may have formulated, furnished, or in any way supplied the said drawings, specifications, or other data, is not to be regarded by implication or otherwise as in any manner licensing the holder or any other person or corporation, or conveying any rights or permission to manufacture, use, or sell any patented invention that may in any way be related thereto.

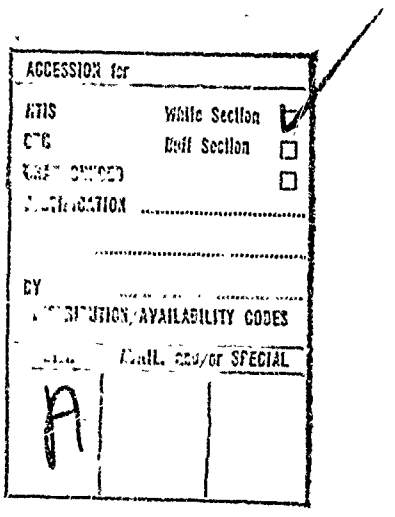


Copies of this report should not be returned unless return is required by security considerations, contractual obligations, or notice on a specific document.

AIR FORCE/56780/27 August 1973 — 100

UNCLASSIFIED

Security Classification

AD-766 444

## DOCUMENT CONTROL DATA - R & D

*(Security classification of title, body of abstract and indexing annotation must be entered when the overall report is classified)*

1. ORIGINATING ACTIVITY *(Corporate author)*
Advanced Systems Division
Air Force Human Resources Laboratory
Wright-Patterson AFB, Ohio 45433

2a. REPORT SECURITY CLASSIFICATION
Unclassified

2b. GROUP

3. REPORT TITLE
Modeling of the Human Force and Motion-Sensing Mechanisms

4. DESCRIPTIVE NOTES *(Type of report and inclusive dates)*
Final Report November 1971 - June 1972

5. AUTHOR(S) *(First name, middle initial, last name)*
Don R. Gum

| 6. REPORT DATE | 7a. TOTAL NO. OF PAGES | 7b. NO. OF REFS |
|---|---|---|
| June 1973 | ~~86~~ 92 | 0 |

| 8a. CONTRACT OR GRANT NO. | 9a. ORIGINATOR'S REPORT NUMBER(S) |
|---|---|
| b. PROJECT NO. 6114 | |
| c. Task: 6114-07 | 9b. OTHER REPORT NO(S) *(Any other numbers that may be assigned this report)* |
| d. Work Unit: 6114-07-05 | AFHRL-TR-72-54 |

10. DISTRIBUTION STATEMENT
Approved for public release; distribution unlimited.

| 11. SUPPLEMENTARY NOTES | 12. SPONSORING MILITARY ACTIVITY |
|---|---|
| | Advanced Systems Division<br>Air Force Systems Command<br>Wright-Patterson AFB, Ohio 45433 |

13. ABSTRACT

The purpose of the study was: to investigate human force and motion-sensing mechanisms; to develop models for the prominent or potentially artificially stimulatable mechanisms; to implement them on an analog computer; and to investigate their responses to various force and motion-forcing functions. Models were implemented and tested for a semicircular canal, the otolith, head motion muscle spindle sensing, and body seat pressure sensing. The relative magnitude of the sensed force and motion through the various mechanisms has not been possible to assess because the action of some mechanism transducers, i.e., the Pacinian receptors, and the processing of the information received from the various receptors is not well understood. However, tests of the models have demonstrated the relative time delays between applied force and perceived force for the various mechanisms, showing that both the muscle spindle and pressure-sensing mechanisms perceive an applied force much more rapidly than the vestibular system. Also, the long adaptation phenomenon associated with the semicircular canals which seems to degrade their usefulness in flight and the rapid adaptation phenomenon associated with the pressure sensors which makes them important sensors for consideration in the design of motion systems have been shown through model testing.

DD FORM 1 NOV 65 1473

UNCLASSIFIED

Security Classification

| 14. KEY WORDS | LINK A | | LINK B | | LINK C | |
|---|---|---|---|---|---|---|
| | ROLE | WT | ROLE | WT | ROLE | WT |
| Motion Simulation<br>Sustained "g" Simulation<br>Physiological Modeling<br>Simulation | | | | | | |

*U.S.Government Printing Office: 1973– 758-425/29

AFHRL-TR-72-54

# MODELING OF THE HUMAN FORCE AND MOTION-SENSING MECHANISMS

*DON R. GUM*

12

## FOREWORD

This report summarizes the results of a study conducted by the Simulation Techniques Branch of the Advanced Systems Division under Project 6114, "Simulation Techniques for Air Force Training", Task 611407, "Mathematical Models and Programming Techniques for Aircrew Training Simulation". The Task Scientist was Don R. Gum. This study was performed during the period of November 1971 to June 1972.

This technical report has been reviewed and is approved.

GORDON A. ECKSTRAND, PhD
Director, Advanced Systems Division
Advanced Systems Division
Air Force Human Resources Laboratory

## ABSTRACT

The purpose of the study was: to investigate human force and motion-sensing mechanisms; to develop models for the prominent or potentially artificially stimulatable mechanisms; to implement them on an analog computer; and to investigate their responses to various force and motion forcing functions. Models were implemented and tested for a semicircular canal, the otolith, head motion muscle spindle sensing, and body seat pressure sensing. The relative magnitude of the sensed force and motion through the various mechanisms has not been possible to assess because the action of some mechanism transducers, i.e., the Pacinian receptors, and the processing of the information received from the various receptors is not well understood. However, tests of the models have demonstrated the relative time delays between applied force and perceived force for the various mechanisms, showing that both the muscle spindle and pressure-sensing mechanisms perceive an applied force much more rapidly than the vestibular system. Also, the long adaptation phenomenon associated with the semicircular canals which seems to degrade their usefulness in flight and the rapid adaptation phenomenon associated with the pressure sensors which makes them important sensors for consideration in the design of motion systems have been shown through model testing.

# SUMMARY AND CONCLUSIONS

## Problem

The approach commonly followed for developing motion simulation requirements and resulting motion systems might best be called the "Duplicative" approach. This approach leads to a motion system's performance requirements, up to its duplicative limits, being derived primarily from the performance of the aircraft being simulated with little attention given to the human sensing the force and motion. One of the problems of this approach is that as the simulator's duplicative capability is increased the cost increases in a much greater than linear relationship. Also there may be characteristics of the human sensing mechanisms which would allow simpler stimulation to produce the sensations of flight which are not being considered and used to advantage.

## Approach

The approach followed during this study was to concentrate on the human by examining his force and motion-sensing mechanisms from a control systems point of view. The sensing mechanisms considered were: the semicircular canals, the otolith, head motion muscle spindle sensing, and body seat pressure sensing. Models of these four mechanisms have been implemented and investigated in much the same manner as a control system engineer examines the dynamic characteristics of sensors in a feedback control system.

## Results

Based on the performance of models when excited by the various inputs, the following comments and conclusions are offered:

1. For man in flight the components of the vestibular apparatus, semicircular canals and otolith, do not seem to be very reliable or useful force and motion-sensing mechanisms. Due to the sluggishness of response of the otolith, its input to the central nervous system is probably the last received. The semicircular canals are also comparatively sluggish in response. Furthermore, an adaptation phenomenon

causes apparent false cues many seconds after a stimulus has been removed. In addition, the vestibular apparatus is rather loosely coupled to an aircraft through body movement, a flexible torso, and a pivoting head.

2. The displacement of body extremities such as the head seem to be very responsive and reliable force-sensing mechanisms. The form of the force-sensing signal closely resembles the applied force. Since there does not appear to be any significant adaptation phenomenon associated with this sensing mechanism, it is probably the most important mechanism to consider for simulating sustained accelerations.

3. The pressure-sensing mechanism seems to be very important for flight in an aircraft due to the fact that there is little delay between applied force and perceived pressure; the adaptation is rapid--enhancing the detection of force changes; and it is directly coupled through the seat to the aircraft. The rapid adaptation phenomenon of the pressure sensors is most likely the reason that present motion systems that provide only onset accelerations, which are removed below the threshold level, work so well.

## Conclusion

What has been learned through this study among other things is that this is definitely a viable approach to the development of improved force and motion simulation devices for pilot training. However, this is just a start with much work remaining to be done in terms of collecting additional experimental data on the two sensing mechanisms for which models have been developed during this study, to verify or refine the models, and better qualify their performance.

TABLE OF CONTENTS

LIST OF ILLUSTRATIONS

# SECTION I
# INTRODUCTION

The study of human force and motion sensing was undertaken with a specific area of application in mind. This area of application is aircraft flight simulation for pilot training. Flight simulators are used extensively today by both the armed services and commercial airlines. The benefits of flight simulators are not limited only to the most obvious--that of reducing the cost of pilot training by reducing the actual aircraft time used in training. Simulators help considerably to reduce the airspace congestion problem and, of course, provide a safe means of training for flight regimes and emergency situations which may be extremely hazardous to perform in the aircraft.

Present-day aircraft simulators, in use or being developed, employ many highly sophisticated forms and devices of artifice. One such device is the simulator motion system which is comprised principally of: (1) a movable platform upon which the simulator cockpit is mounted and (2) appropriate motion system drive software and computation. The job of the motion system is to duplicate, within a relatively small confined volume, the motion and force sensations normally imparted to a pilot by an aircraft as it consumes miles of airspace. While some existing motion simulators are satisfactory for certain classes of aircraft, they are quite inadequate for others. For large slow dynamics aircraft or those flown in an environment of force varying only slightly above and below one "g" at limited pitch and roll attitudes, the simulation of motion, in a way that is seemingly acceptable to pilots, is within the state-of-the-art (Reference 1). However, for aircraft that are very responsive and are flown in air-to-air combat or aerobatic flight regimes, adequate motion simulation devices are not available.

In trying to develop or determine adequate motion simulation for the various flight regimes including the more extreme flight environments, three diverse directions of approach are possible. The first, which might be called the "duplicative" approach, leads to a motion system's performance requirements, up to its duplicative limits, being derived primarily from the performance of the aircraft being simulated, with little attention given to the human sensing the force and motion This seems to be the popular approach today. This is to be expected since the kinetics of flight are widely known and relatively easy to describe mathematically; whereas, some of the human force and motion-sensing mechanisms have only recently been expressed analytically and others not addressed at all.

For a ground-based simulator the "duplicative" approach amounts essentially to the duplication of the onset of forces and motions which are then removed at the subliminal level. The extreme of the approach would be total inflight simulation where one aircraft is used to simulate another. The principle drawback of this approach is that, as the simulator's duplicative capability increases, the cost increases rapidly, negating the primary advantage of simulators.

The second approach is to look at the human in terms of how he senses force and motion, and to develop, if possible, artificial means for stimulating these sensing mechanisms. This would be more of a "true simulation" approach.

The third approach, which would be best termed the "empirical" approach, involves using a "duplicative" motion system with the greatest capabilities available, implemented in such a manner that its capabilities can be systematically degraded. The motion system would then be used for empirical transfer of training studies with groups of pilots to determine the kind and extent of force and motion necessary to successfully

and efficiently train pilots. The primary hazards of this approach are that the capabilities of the motion system available may not be adequate to start with and that it does not consider artificially stimulative means.

The objectives of the three diverse directions of approach can be summarized with the following questions: What does the aircraft to be simulated do? Does the pilot sense it and how? If so, is it necessary for him to sense it in order to learn to fly the aircraft? Obviously all three directions of approach are interrelated and none can be followed singly if the optimum motion simulation system for a particular aircraft and training program is to be developed.

The objective of this study was essentially to look at the human to see what sensing mechanisms are involved, investigate those that appear to be the prominent mechanisms and those that are potentially artificially stimulatable, and determine which are the most sensitive or responsive. This objective has been accomplished by examining the human force and motion-sensing mechanisms from a control system point of view. Models of four force and motion-sensing mechanisms have been implemented and investigated in much the same manner as a control system engineer examines the dynamic characteristics of sensors in a feedback control system.

## SECTION II
## FORCE AND MOTION-SENSING PHYSIOLOGY AND MODELING

The initial investigation into the force and motion sensing area considered several mechanisms through which the body experiences force and motion. The initial list included: (1) the vestibular system (semicircular canals and otolith); (2) sensations due to displacement of body extremities such as limbs and the head; (3) body pressure sensing through contact with an object such as a seat; (4) the movement of fluids in the body causing dilatation and deformation of body organs and fluid-carrying vessels; (5) the displacement of body organs; and (6) the slumping of the fleshy parts of the body. Mechanisms 4 and 5, fluid movement and body organ displacement, being internal to the body, were eliminated from further consideration since artificial means of stimulation appear to be impossible without being deleterious to the subject's health and well-being. The same might be said for the semicircular canals and otolith; however, since they appear to be the primary force and motion-sensing mechanisms of the body--at least for man in his natural environment--they definitely warrant consideration. Also, since mechanism 6 is most likely sensed through a combination of the same sensors imbodied in mechanisms 2 and 3, it was not considered.

The models used or developed were limited to those shown in Figure 1: a semicircular canal, the otolith, head motion/neck muscle spindle, and seat pressure. Furthermore, the modeling was limited to those components of the sensing mechanisms that would be stimulated in a pilot from angular acceleration about the vertical axis and linear acceleration along the lateral axis of an aircraft. The lateral aircraft dynamics used for the combined model testing, shown in Figure 1, were the short-period phugoid response of a typical fighter type aircraft. This forcing function was essentially an underdamped sinusoid exciting all of the models.

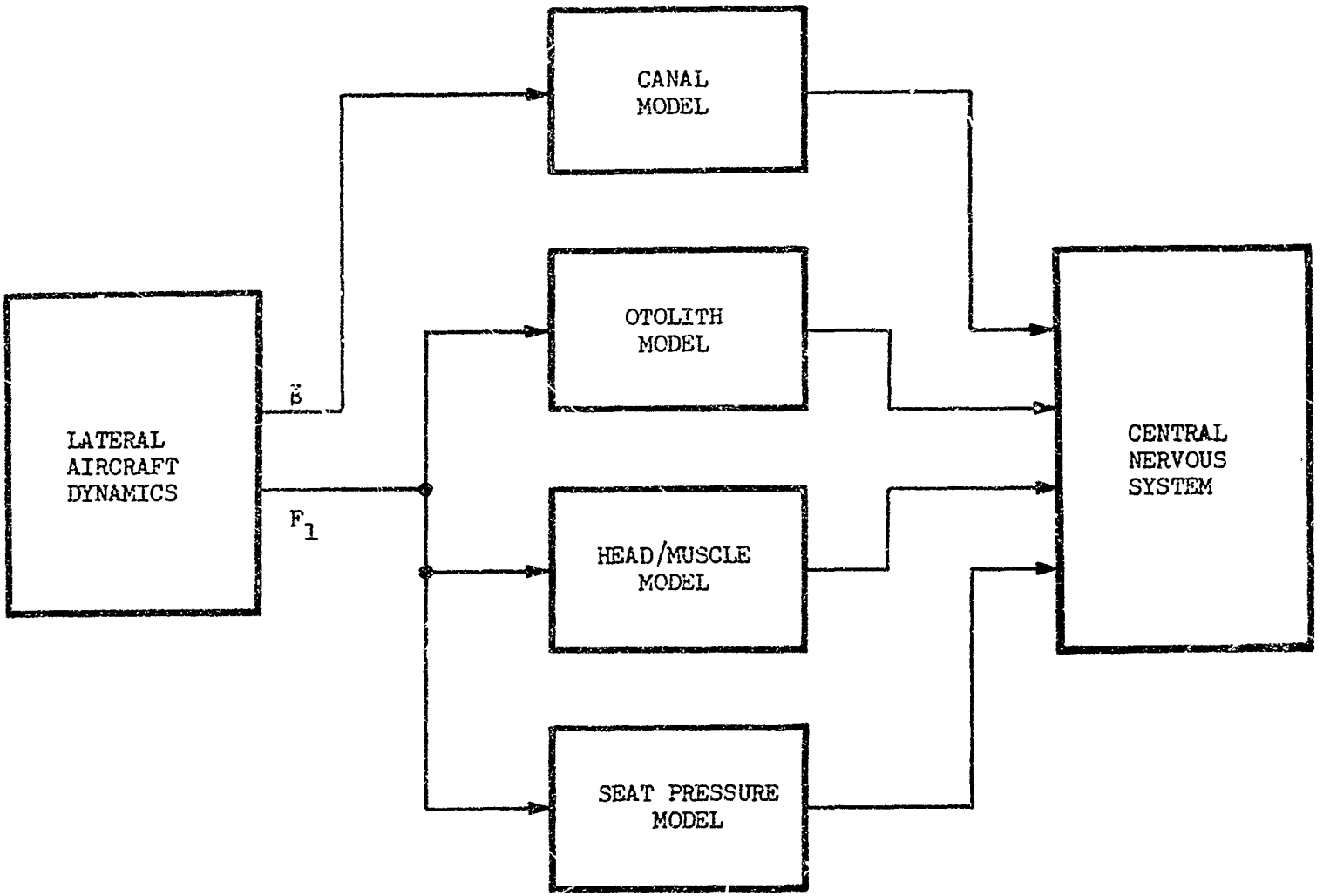


Figure 1. Composite Force and Motion Sensing Model

## THE VESTIBULAR SYSTEM

The vestibular apparatus, or what is referred to as the membranous nonauditory labyrinth, is composed of two sacs--the saccule and the utricle--and three semicircular canals. There are two vestibular apparatuses, one located in each internal ear within the petrous part of the temporal bone. The delicate membranous chambers of the membranous labyrinth are enclosed within corresponding bony cavities. Figure 2 depicts the actual form of the membranous nonauditory labyrinth and its orientation with respect to the head. Figure 3 is a schematic sketch showing the physical arrangement and functional parts.

Each vestibular apparatus consists of two sets of motion sensors, one angular and one linear, called the semicircular canals and the otolith, respectively. The angular sensors, which sense both angular acceleration and velocity, but primarily angular velocity in their mid-range of operation, consist of three semicircular canals which lie in three mutually perpendicular planes. They are named according to their orientation as superior, posterior, and horizontal. Each canal forms about two-thirds of a circle, one end of which is dilated and called the ampulla. They are slightly compressed from side to side, and their diameter is from 0.15 to 0.3 mm with the diameter of the ampulla being 1.2 to 2.4 mm (References 2 and 3). They open into the vestibule by five aperatures only, since the medial end of the superior canal joins the upper end of the posterior canal to form a common canal called the crus commune. The vestibule is the middle portion of the membranous labyrinth which connects from behind with the semicircular canals and in front with the cochlea. The cochlea is the auditory portion of the membranous labyrinth.

The superior semicircular canal is from 15 to 20 mm in length and is situated nearly vertical (Reference 4). Its ampullated end opens

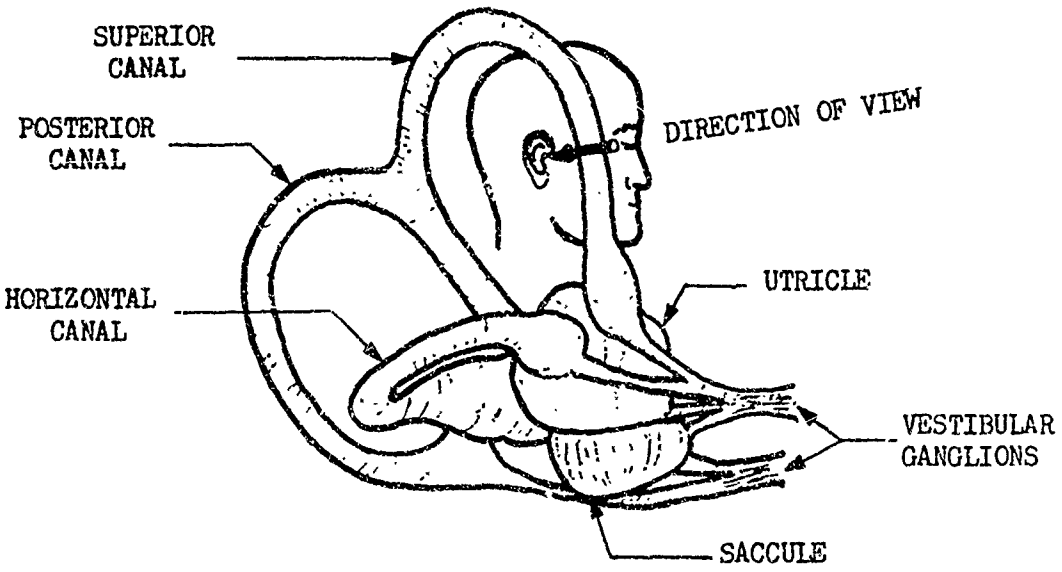


Figure 2. Membranous Nonauditory Labyrinth
(Partially redrawn from Hardy, 1934)

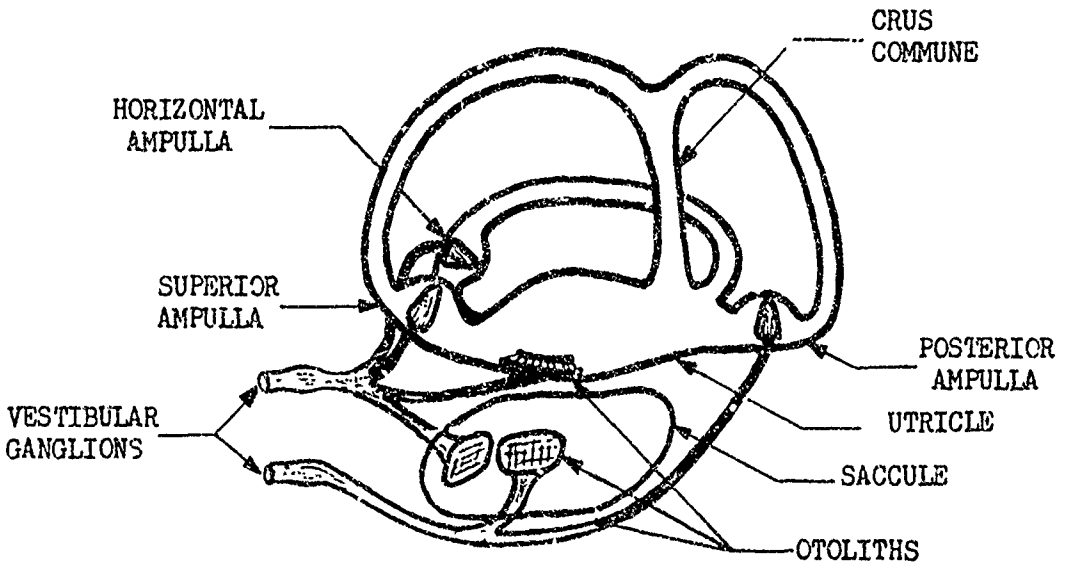


Figure 3. Schematic Sketch of the Vestibular Apparatus
(Partially redrawn from de Burlet, 1924)

into the vestibule immediately above the ampullated end of the horizontal canal. Its opposite end joins the nonampullated end of the posterior canal to form the crus commune which is about 4 mm long and opens into the upper part of the vestibule. The posterior semicircular canal is from 18 to 22 mm in length and is also situated nearly vertical. Its ampulla opens into the rear part of the vestibule. Its upper end joins the crus commune. The horizontal canal is from 12 to 15 mm long and is located about 30° from horizontal. Its ampullated end opens into the vestibule close to the ampullated end of the superior canal. The orientation of the two sets of canals within the head is shown in Figure 4. The horizontal canals are nearly in the same plane. Also, the superior canal of one set of canals is nearly parallel to the posterior canal of the opposite set.

The semicircular canals which are sensitive to angular velocities and accelerations rely essentially on the inertial movement of the fluid with respect to the canal. Figure 5 illustrates schematically the right and left horizontal canals. The canals as shown in Figure 5 are greatly enlarged beyond their normal size with respect to the size of the head. The arrows in the canals indicate the direction of fluid flow relative to the canal walls for a sudden turning movement of the head to the right. This movement of fluid relative to the canal walls causes the deflection of a fluid-tight flap called the cupula. Figure 6 illustrates a greatly magnified cupula cross section. The upper part is composed of hair endings embedded in gelatinous material. Nerve fibers from below ramify around the hair cells. The deflection of the cupula causes mechanical strains on the hair cells generating neural signals.

The linear acceleration sensor is the otolith which is located in the utricle as shown in Figure 7. The saccule also contains two otoliths as shown in Figure 3. In mammals these two otoliths of the

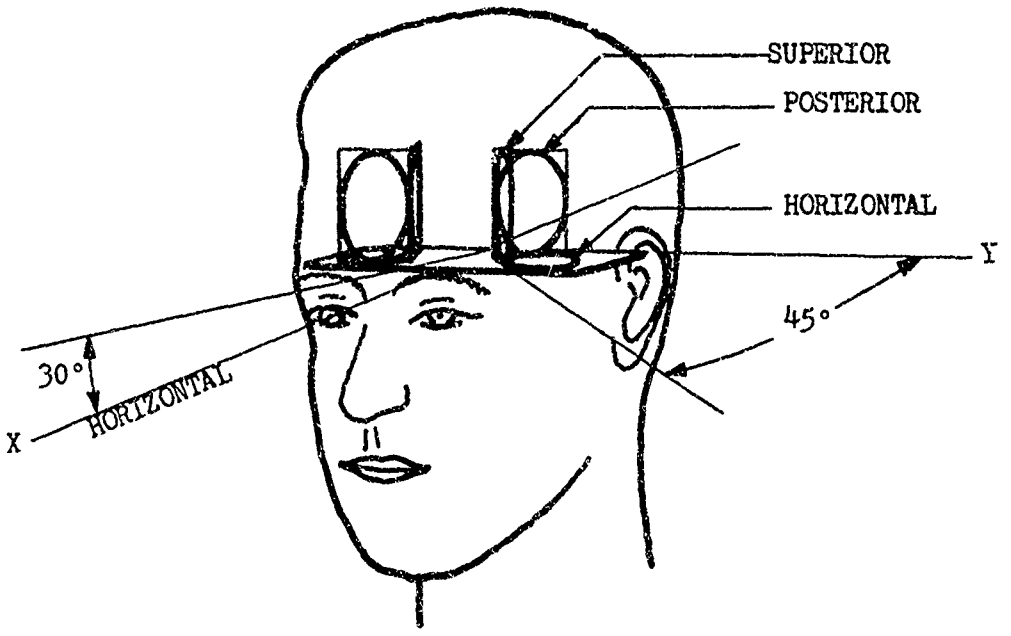


Figure 4. Orientation of Semicircular Canals
(Redrawn from Borlace, 1967)

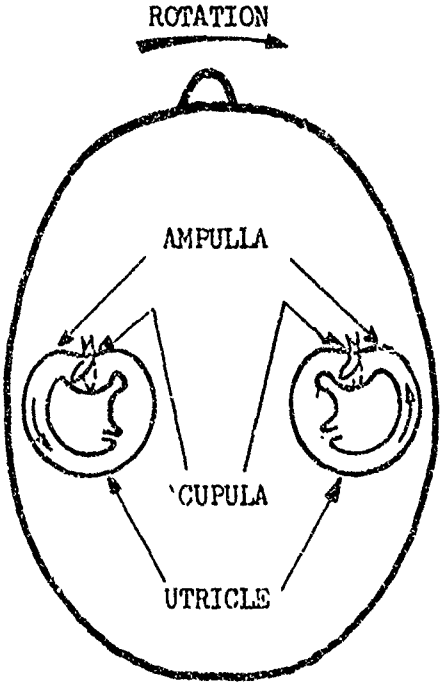


Figure 5. Operation of Horizontal Semicircular Canals

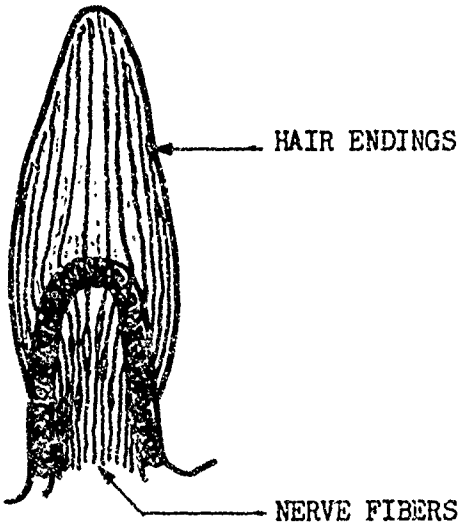


Figure 6. The Cupula of the Crista Ampulla
(Redrawn from Kolmer, 1936)

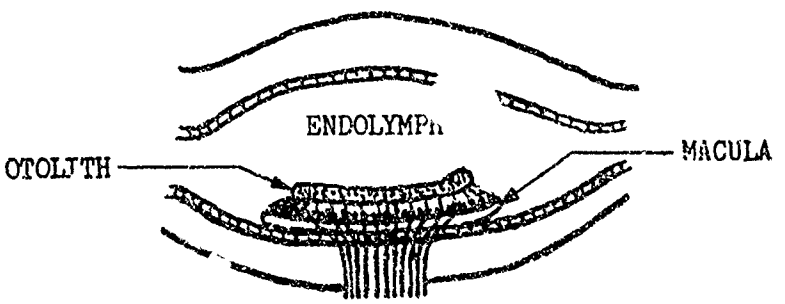


Figure 7. Utricle Section Showing Otolith and Macula
(Partially redrawn from Kolmer, 1936)

saccule occupy two different planes. It was thought at one time that these two otoliths, together with the otolith of the utricle, represented a triplanar linear acceleration sensing system equivalent to the angular acceleration sensing system of the semicircular canals. However, it is unlikely that the saccule and its constituents serve any equilibrium function.

A cross-sectional diagram of the utricle otolith is shown in Figure 8. The actual otolith part is a gelatinous mass containing many calcium carbonate crystals called otoconia. The otoconia give the otolith a density greater than that of the surrounding fluid. The otolith is supported and restrained by hairs and sensory cells. When displaced, it moves with respect to the macula, bending the hair embedded in the sensory cells generating neural signals. The macula is of an oval shape and measures approximately 3 mm in length and 2.3 mm at its greatest breadth. The displacement of the otolith with respect to the macula is limited to approximately 0.1 mm.

The utricle otolith is oriented within the head so as to be able to detect linear acceleration components along each of the three mutually perpendicular axes of the head. The otolith lateral axis corresponds to the lateral or Y-axis of the head. The otolith longitudinal axis is tilted upward by about 30° from the longitudinal or X-axis of the head.

Every normal human has two complete functioning vestibular apparatuses, canals and otolith, a left and a right. Each generates independent asymmetric bidirectional perceived angular velocity and acceleration signals which are summed together synergistically, and linear velocity and acceleration signals which are also summed together synergistically. This summing of both left and right vestibular signals of a common type might be thought of as two separate sensing mechanisms operating in a class AB push-pull manner.

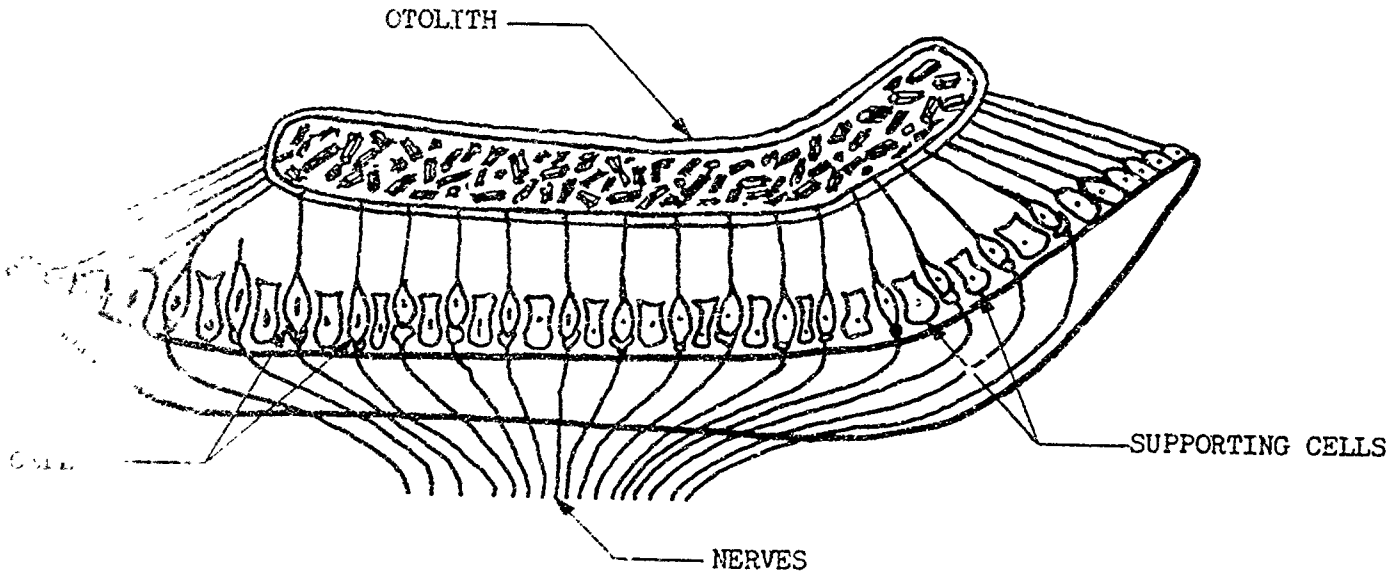


Figure 8. Cross Section of an Otolith and its Macula
(Redrawn from Groen et al., 1952)

The models used for both the semicircular canals and otolith were those developed by Young et al.(Reference 2). The mechanical functioning of each semicircular canal for modeling purposes is considered to be analogous to that of a torsional pendulum. The moment of inertia of such a pendulum is due to the moment of inertia of the fluid, the endolymph, moving in the canal. The small bore of the canal insures laminar flow of the contained fluid so that the resulting viscous flow resistance is almost linearly dependent on velocity. The cupula acting as a weak spring tending to restore itself to a neutral position contributes elastance to the total canal system. Therefore, the input/output relation between skull movement and cupula deflection acts as a second-order system with the components being the fluid inertia, fluid viscous friction, and cupula springiness.

The torsional pendulum transfer function written in Laplace transform notation relating cupula deflection to head angular acceleration is:

$$\frac{d_c(s)}{\ddot{\beta}(s)} = \frac{K}{s^2 + 2\zeta\omega_n s + \omega_n^2}$$

The roots of the denominator are real and widely separated (i.e., the system is very overdamped) and may be rewritten as:

$$\frac{d_c(s)}{\ddot{\beta}(s)} = \frac{K}{(s + a)(s + b)}$$

where: $0.04 < a < 0.2$ radian/second,

$a_{nominal} = 0.0625$ radian/second (lateral canal), and

$4 < b < 300$ radians/second,

$b_{nominal} = 10$ radians/second.

The complete semicircular canal model for perceived angular velocity is shown in Figure 9. The model includes, in addition to the canal dynamics, linear adaptation dynamics, a central processing delay, and a threshold nonlinearity.

Experimental results have shown that the sensitivity of the canals decreases for repeated or continuous stimulus patterns. This phenomenon, called adaptation, concerned investigators for many years and could not be duplicated with the simple torsional pendulum model. To account for this adaptation phenomenon, Young and Oman included linear adaptation dynamics represented by a simple exponential decay with a time constant of 30 seconds. Also included was a pure delay of 0.3 second to account for additional central processing for subjective signals. The nonlinearity or threshold function included in the model with the threshold set to approximately 2°/second accounts for the latency time response of the semicircular canals.

Little or no extensive work has been reported on the modeling of the otolith with the exception of that done by Young et al. (Reference 2). The mechanical functioning of the otolith for modeling purposes is considered to be analogous to an overdamped spring-mass-dashpot linear accelerometer. The otolith, due to its composition being denser than the surrounding fluid, acts as an inertial mass coupled to the skull via the utricle through the viscous friction of the endolymph and the centering elastic hair attached to the macula supporting the otolith.

The spring-mass-dashpot transfer function written in Laplace transform notation relating otolith displacement with respect to its macula to linear acceleration of the head is:

$$\frac{d_o(s)}{F_1(s)} = \frac{K}{s^2 + 2\zeta\omega_n s + \omega_n^2}$$

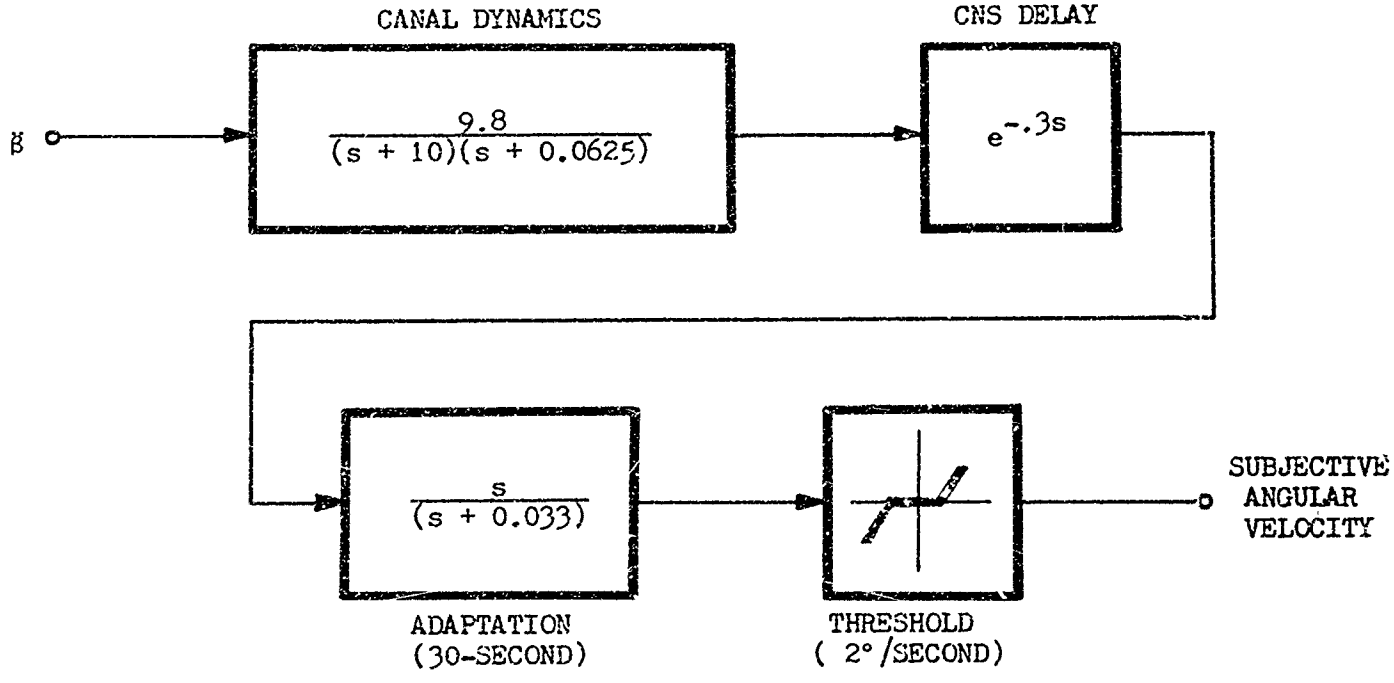


Figure 9. Model of Horizontal Semicircular Canal

The roots of the denominator are real and the system is overdamped and may be rewritten as:

$$\frac{d_o(s)}{F_1(s)} = \frac{K}{(s + a)(s + b)}$$

where: $a_{nominal}$ = 0.19 radian/second and

$b_{nominal}$ = 1.5 radians/second.

The complete otolith model for perceived linear acceleration is shown in Figure 10. The model, in addition to the otolith dynamics, includes a threshold nonlinearity and a neural lead processing function. The nonlinear or threshold function included in the model with the threshold set to approximately 0.005 g accounts for the latency time response of the otolith. The lead term is believed to be due to neurological adaptation or processing of otolith displacement, rather than the mechanics of the otolith structure.

## MUSCLE SPINDLE SENSING

There are sensors of various types which detect motion of the body or its parts and forces applied thereto. Some of these, like those discussed in the vestibular system, indicate orientation and motion of the body with respect to its external environment. Others, however, measure motion and displacement of parts of the body with respect to the body reference frame. It is these sensors located primarily within the skeletal muscles that were of interest in this part of the study. They were of interest not from the standpoint of the voluntary control of a body extremity such as the arm, leg, or head but from the standpoint of how these extremities respond to and how the sensors that are a part of them detect external displacement forces. From a control systems point-of-view, this amounts to how the system which controls

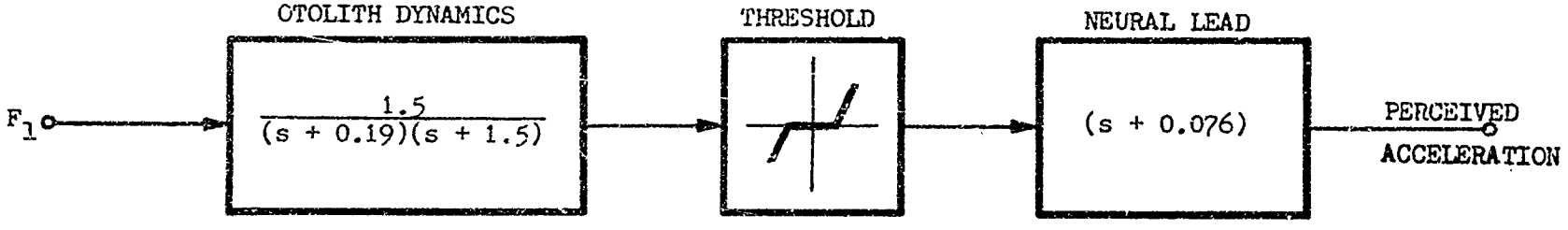


Figure 10. Model of Lateral Component of Otolith

the body extremity position responds and what the characteristics of the feedback signal are for an external disturbance applied to the system load, in this case the mass of the head.

The head was selected as the extremity to be investigated and modeled since it is the least restrained of all the large extremities for a pilot seated in an aircraft. Motion of the head was limited to that about the longitudinal axis and the head was considered to be sitting on a rigid spinal column pivoted about the first cervical. Since the center of gravity of the head is above the pivot point, the head behaves like an inverted pendulum whose angular position with respect to the body is controlled by the neck muscles. There are numerous muscle pairs in the neck to control head movement; however, the sternocleidomastoideus, as shown in Figure 11, is the primary muscle pair for controlling head rotation about the longitudinal axis. The sternocleidomastoideus muscle derives its name from the fact that it connects to the skull in the mastoid area, runs down the neck and divides, with the larger part attaching to the clavicle and the smaller part attaching to the sternum.

The basic component of a muscular control system is striated muscle, which is a unidirectional, force-generating mechanism. Muscle pairs such as the sternocleidomastoideus muscles of the neck, innervated by alpha motor neurons in the spinal cord, work together and against each other to provide position, velocity, and force control of the head. Also, sensory mechanisms within the muscles send signals to the central nervous system for controlling the voluntary motor activity.

The muscles themselves are composed of numerous muscle fibers extending the entire length of the muscle with all of the fibers roughly parallel in orientation. A single muscle fiber is, in turn, subdivided into several thousand parallel units called myofibrils. The

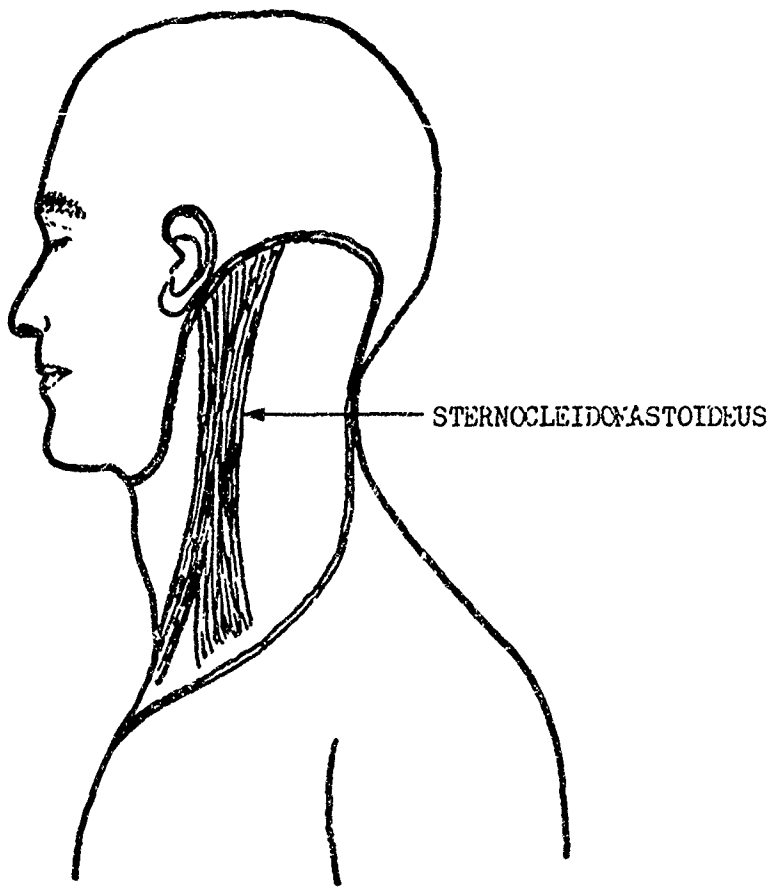


Figure 11. The Sternocleidomastoideus Muscle

mechanisms of contraction lie within the tiny myofibrils. A number of muscle fibers are innervated by a single motorneuron and thereby always act in unison. This group of fibers is termed a motor unit, thus forming the basic functional unit of muscular contraction. The total force generated by a muscle is the summation of tension developed by each of the motor units within the muscle.

In modeling the muscle it is considered as a single force-generating unit. The variables affecting muscle force output are: activation level, instantaneous muscle length, and shortening velocity of the muscle. The commonly accepted lumped parameter model used to describe muscle dynamics (Reference 5) is shown in Figure 12. The additional elastic element, $K_s$, in series with the force generator is attributable to tendon and connective tissue. The transfer function for this model is approximately:

$$\frac{F}{\Delta f}(s) = \frac{K_f}{1 + \frac{B_m}{K_s} s}$$

Where: F is the output force,

$\Delta f$ is small changes in activation level,

$B_m$ is muscle damping,

$K_f$ is the muscle force constant,

$K_s$ is tendon easticity and

$K_s >> K_m$.

For large stimulus rates the time constant, $T_m = \frac{B_m}{K_s}$, for a slow skeletal muscle ranges from 50 to 100 milliseconds (Reference 6).

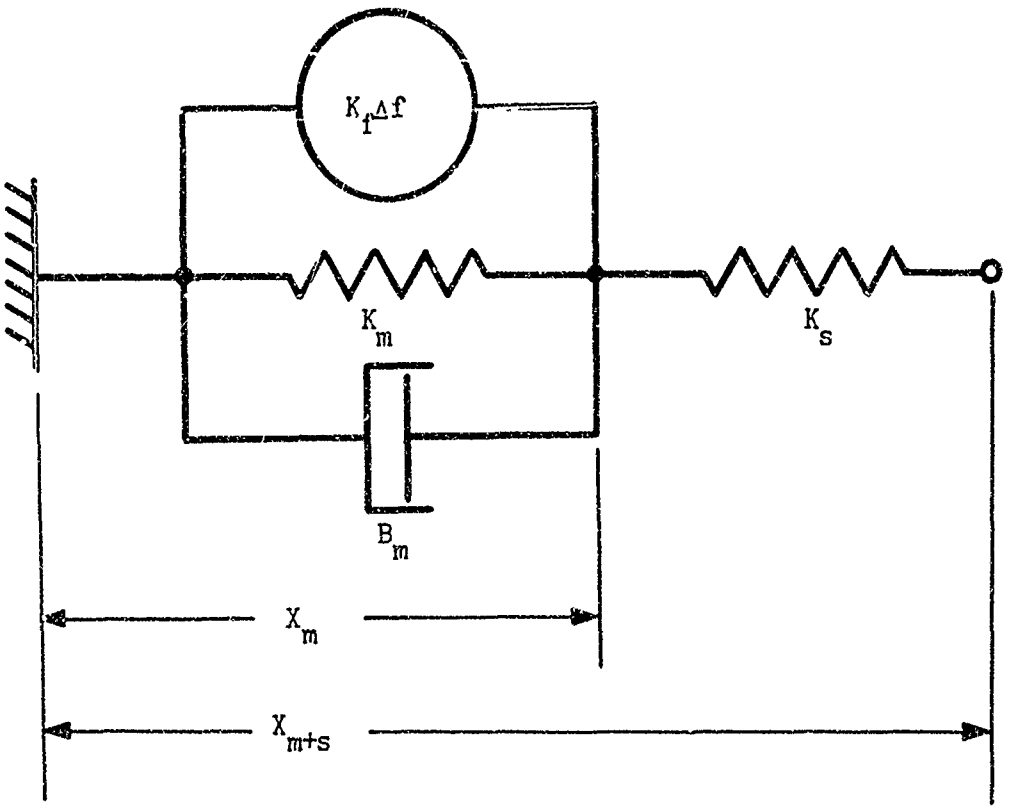


Figure 12. Lumped Parameter Muscle Model
(Redrawn from Stark, 1966)

The muscle length receptors which are called muscle spindle receptors are several centimeters in length and are interspersed throughout the muscle. Muscles involved in fine control have more receptors per unit weight than those performing coarse movements. These receptors supply the central nervous system with signals related to the position and velocity of the muscle in which they are located.

Located in parallel with the main muscle fibers are a few fibers called intrafusal fibers of two types, nuclear bag and nuclear chain fibers. Shown in Figure 13 is an exaggerated diagram of a bundle of intrafusal fibers. The afferent innervations, those sending information to the central nervous system, include two types of endings, primary or annulospiral endings and secondary or flower spray endings. The primary endings are sensitive mainly to rate of change of muscle length. The secondary endings sensitive to muscle length are less abundant than the primary, and the nerve endings which relay their messages to the central nervous system are somewhat slower.

The intrafusal fibers are also innervated by small $\gamma$-efferents, those bringing control information to the muscle, which are of two types, plate endings and trail endings. The $\gamma$-efferents are separated into two groups, $\gamma$-dynamic and $\gamma$-static fibers; however, there is no consistent relationship between functional and anatomical definitions. Increased $\gamma$-dynamic activity increases the velocity sensitivity of the primary afferent response and changes in $\gamma$-static activity vary the bias discharge levels in the responses of both the primary and secondary afferents.

As reported by Nashner (Reference 7), several investigators have developed models for the primary afferent response of the muscle spindle. The basic model is of the general form:

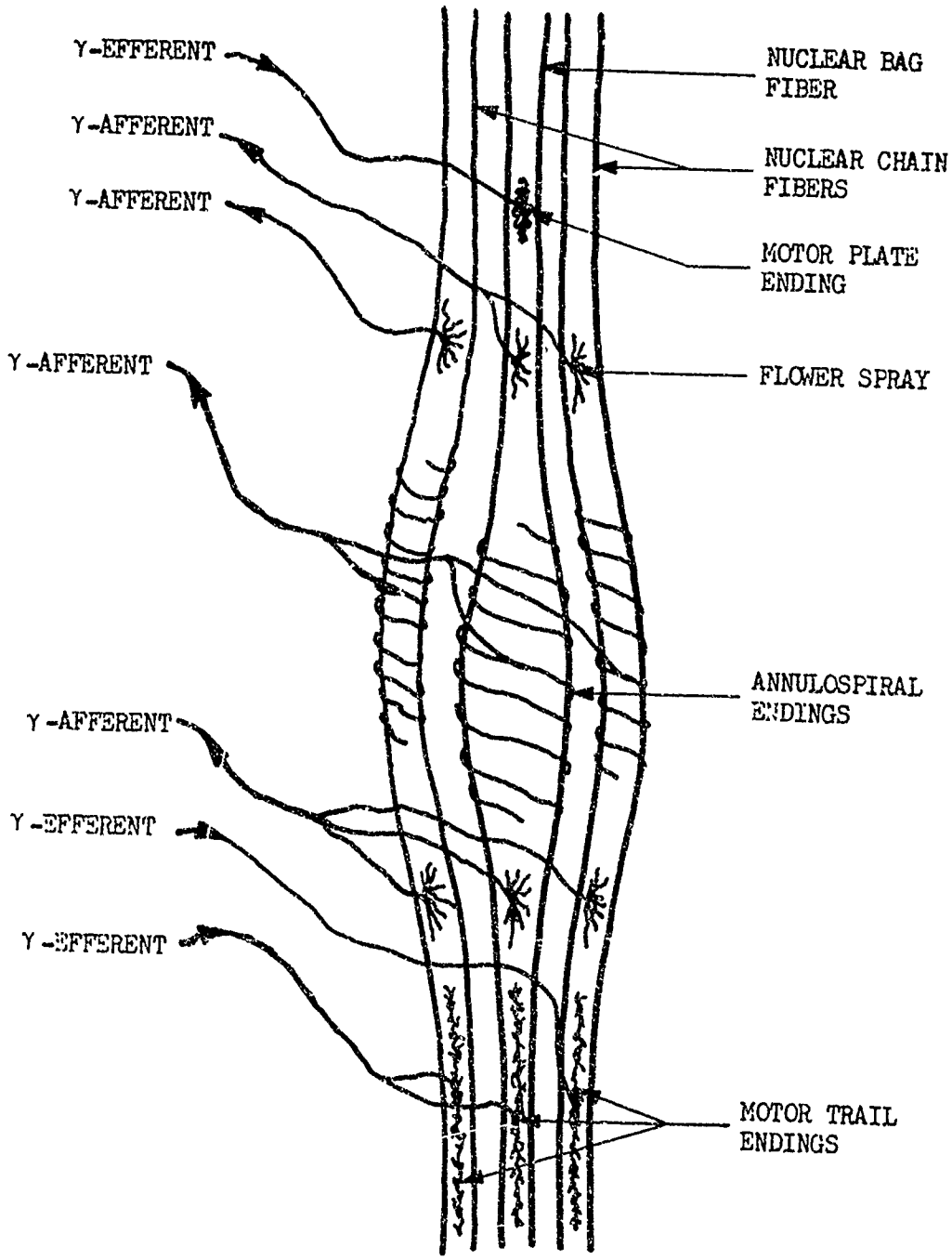


Figure 13. Muscle Spindle Diagram
(Redrawn from Nashner, 1970)

$$f(s) = \frac{K(T_1 s + 1)}{(\alpha T_1 s + 1)(T_2 s + 1)} X_m(s)$$

where: $f(s)$ is the output firing rate,

$X_m(s)$ is the muscle spindle length, and

$K$ is the muscle spindle gain.

The parameters for this model necessary to match step response data from Lippold et al. (Reference 9) were found by Agarwal et al. (Reference 10) to be approximately:

$T_1$ = 0.28 second,

$T_2$ = 0.0055 second, and

$\alpha$ = 0.21

They show that a "lead-lag" model, as shown below, is adequate to predict the basic form for the muscle spindle response to stretch inputs.

$$f(s) = \frac{K(T_1 s + 1)}{(\alpha T_1 s + 1)} X_m(s)$$

Based on the models for the muscle, muscle spindle, and the mechanics of head movement, a lateral head position control system model was developed. For this model the upper part of the spinal column or neck was considered to be rigid with the head p voted about the first cervical. The head with its center of gravity above the pivot point has its lateral angular motion controlled primarily by two major neck muscles, the sternocleidomastoideus, working as an agonist/ antagonist pair.

A diagram of the mechanical aspects of the head control system is shown in Figure 14. The following torque equation describes the motion:

$I_h$ is the moment of inertia of the head about the neck pivot,

$B_n$ is the damping due to other muscles and neck tissue not involved in active motion,

$K_n$ is the elastance due to other muscles and neck tissue not involved in active motion,

$M_h$ is the mass of the head,

r is the distance from the pivot to the center of mass,

g is the acceleration due to gravity and

$\theta$ is the displacement angle.

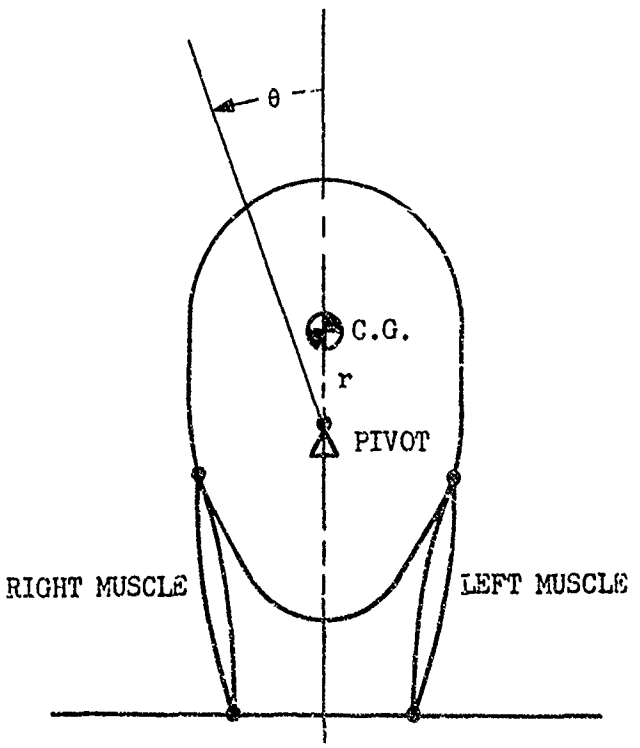


Figure 14. Head/Muscle System

Since the angular displacement of the head is limited to approximately ±20°, a small angle approximation of sin $\theta = \theta$ was used in the model. Also, only operation in the unlimited or linear range was considered. The head motion equation rewritten including this simplification is:

$$\frac{d^2\theta}{dt^2} = -\frac{B_n}{I_h}\frac{d\theta}{dt} - \frac{K_n}{I_h}\theta + \frac{M_h g\, r}{I_h}\theta + \frac{T_n}{I_h}$$

The equation for the torque applied to the head by the muscles is:

$$T_n = d\,F_r - d\,F_l$$

where: $d$ is the perpendicular distance from the head pivot point to the muscle and

$F_r$ and $F_l$ are the forces generated by the right and left sternocleidomastoideus muscles respectively.

The control system model diagram for lateral head motion control is shown in Figure 15. The inner positive feedback loop is the gravity influence which tends to pull the head from its righted position.

The following are values which were used in the model:

Head

$M_h$ = 4.6 kilograms

$I_h$ = 0.0304 kilogram meter$^2$

$\omega_n \simeq$ 7.81 radians/second

$\zeta \simeq$ 0.64

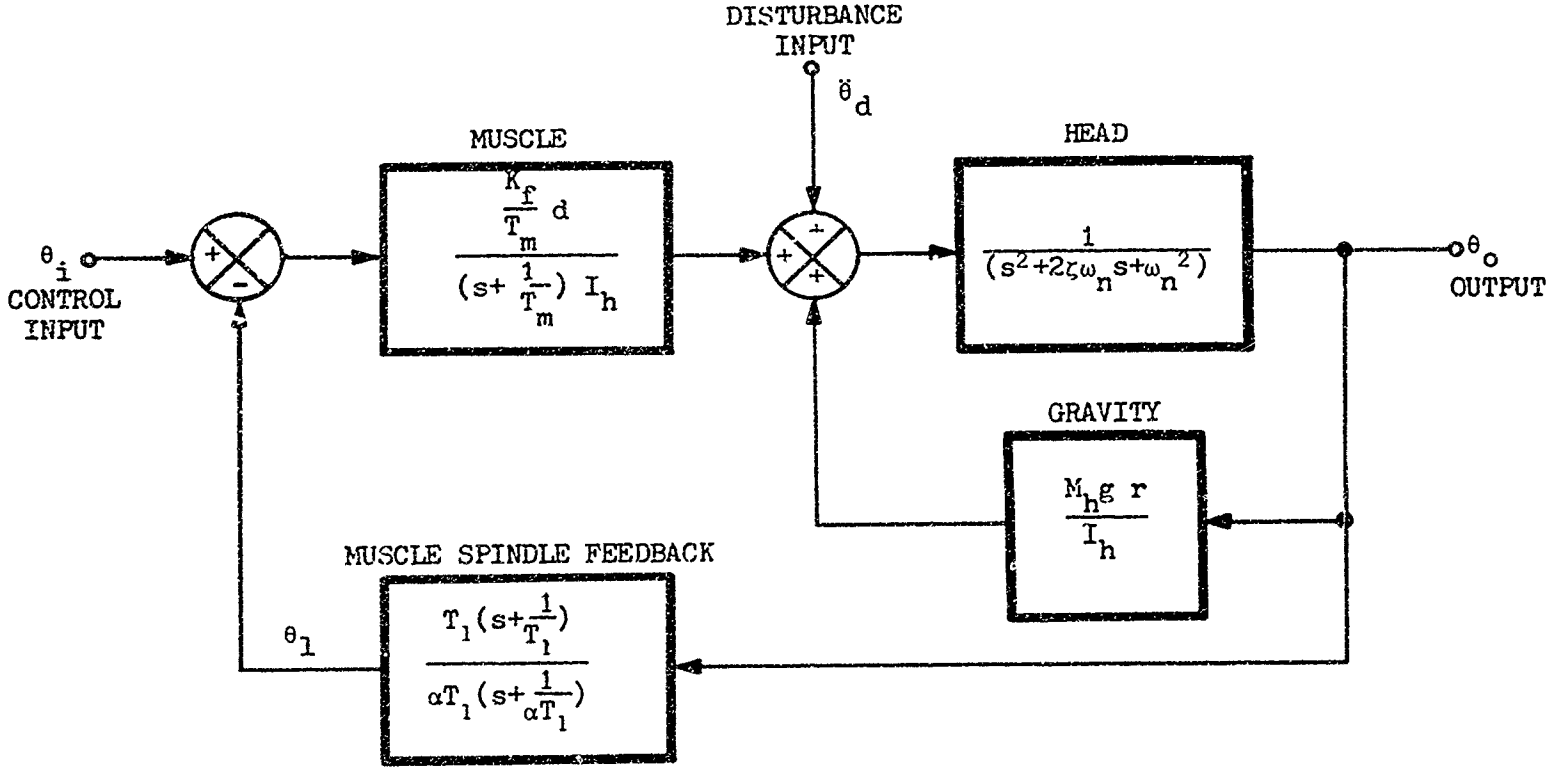


Figure 15. Lateral Head Motion Control System

Gravity Torque

$$\frac{M_h g\, r}{I_h} = 73.8 \quad 1/\text{second}^2$$

Muscle Force

$$F_{r_{max}} = F_{l_{max}} = 43 \text{ newtons}$$

Muscle

$$K_f = 43 \text{ newtons}$$

$$d = 0.075 \text{ meter}$$

$$T_m = 0.08 \text{ second}$$

$$\frac{T_n}{I_h} = \frac{1640}{(s + 12.5)} (\theta i - \theta i)$$

Length Feedback

$$T_l = 0.25 \text{ second}$$

$$\alpha = 0.20$$

$$\theta_l = \frac{5(s + 4)}{(s + 20)}$$

The data on head mass was taken from Reference 8. Data could not be found for the moment of inertia of the head about the longitudinal axis; therefore, it was calculated using a head model made up of two regular geometric shapes (see Appendix B). The head model natural frequency and damping data were chosen to make the head model match performance data taken from a single subject. The data for maximum muscle force was calculated from roughly measured data on the same subject. The muscle time constant value was based on data from Reference 6, and the muscle spindle values approximate data from Reference 10.

## BODY PRESSURE SENSING

The third type of force and motion-sensing mechanisms considered in the study were those which produce sensations due to the body being in contact with an external object. Of primary interest were the pressure receptors which produce neural signals when the body is deformed slightly by having pressure applied to it by an object such as a seat. The buttocks area was chosen since it is the largest load-carrying area in contact with the seat for a pilot flying an aircraft.

Various types of receptors or free nerve endings are found in the skin, the serous membranes of the heart, and blood vessels, as well as in smooth and striated muscle (Reference 11). These receptors are preferentially sensitive to light touch, deep pressure, or pain. The encapsulated nerve endings are found in a variety of shapes and sizes and each has specific functional properties attributed to it. These receptors are believed to transform physical energy into chemical changes which produce specific irritation of free nerve endings and cause nerve impulses. The most representative example of an encapsulated receptor, and the one of primary interest here, is the Pacinian corpuscle. It is found primarily in the periosteum, ligaments, subcutaneous tissue, many viscera walls, and internal organs. This receptor which senses pressure consists of a free nerve ending surrounded by a thick laminated capsule. The ellipsoid shaped structure sometimes contains more than 30 layers of concentrically arranged fibers, separated by layers of fattened lamellar cells. The Pacinian corpuscles are approximately 0.5 mm along the major axis of their ellipsoidal shape.

Little quantitative data describing the transfer function characteristics of the pressure receptors could be found. Nothing

seems to be available to indicate linearity or dynamic range of pressure discrimination. Also, little seems to be known about how the outputs of the individual receptors are combined to integrate the perception of pressure applied to the body.

According to Strughold (Reference 12), the specific stimulus for the pressure sensory nerves is not only pressure as such but also change in pressure. The intensity of the sensations aroused depends on the degree, as well as the rapidity of the deformation. Also once deformed, as a steady-state condition, such as a pilot sitting, the body pressure sensors seem to respond more intensely to further deformation than they do to a reduction in deformation. Strughold also suggests that there is a rapid adaptation process where the sensations to prolonged pressure fade rapidly so that new changes in pressure are readily sensed. No quantitative information regarding this adaptation process is given except that it is much more rapid than the vestibular apparatus and may be around one second.

The minimum energy required for the stimulation of a pressure point seems to be much less significant than the discrimination thresholds. The relative discrimination threshold is about 3.4% during stressing; that means that two forces must differ by at least this amount to produce sensations of different intensity (Reference 12). During destressing the threshold is approximately 6.5%. The latent time of the sensation ranges between 35 and 100 milliseconds, which means that the pressure-sensing mechanism reacts very rapidly. Strughold emphasizes the importance of the pressure sensors and seems to indicate that they may be more useful to pilots in flight than the vestibular apparatus. He further recommends increasing the contact area between the pilot and his aircraft.

The above information suggests a model as shown in Figure 16. The body pressure dynamics are for a human subject sitting on a

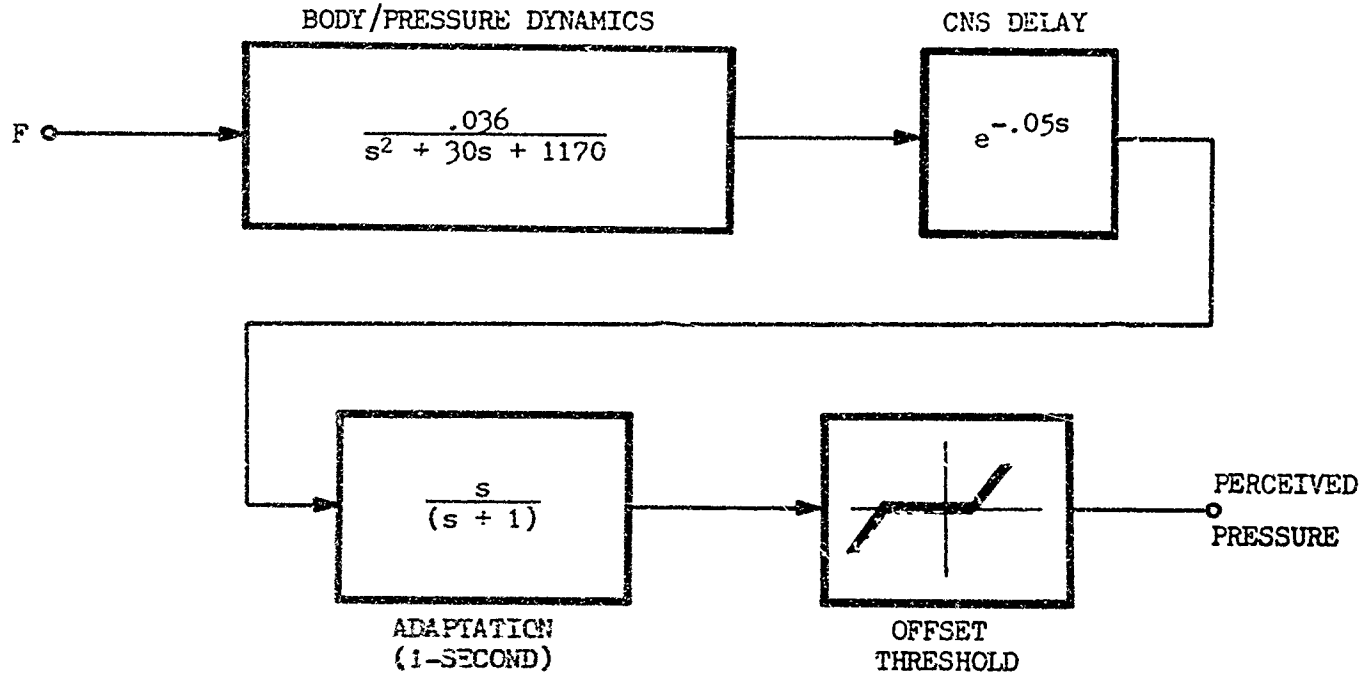


Figure 16. Body Pressure Sensing Model

nonflexible surface. The second block is a pressure perception delay, the third block is the adaptation part of the model, and the fourth block is an offset threshold function, favoring positive or stressing pressures.

The physiology and modeling work from this point are concentrated on the area of the body receiving the pressure and the dynamics involved. In researching the past work devoted to developing data relevant to the pressure distribution on the buttocks area, it was found ironically that this work was done primarily for the purpose of developing more comfortable aircraft seats, thereby minimizing the seat pressure sensations received by the pilot.

Figure 17 shows a cutaway view of a human seated on a seat cushion. Due to the structure of the body, man in the seated position is largely supported through the fleshy part of the buttocks by two lower protrusions of the pelvis called the ischial tuberosities. The pressure on the tuberosity areas is extremely high, being over forty times the average buttocks pressure of approximately 700 newtons/meter$^2$ (References 13 and 14).

The approximate pressure distribution for the buttocks area, which was redrawn from Hertzberg (Reference 14) and converted to MKS units, is shown in Figure 18. The data reported by Hertzberg were taken from unpublished work by Dempsey. Based on the data showing that the areas under the tuberosities are the greatest areas of pressure, a body/buttocks/seat model, as shown in Figure 19, was developed. Due to symmetry, only one-half of the model need be considered, as shown in Figure 20. Figure 21 shows the mechanical circuit diagram for this model for which the system differential equations are:

$$f = M_b \frac{d^2X_b}{dt^2} + B_b \left(\frac{dX_b}{dt} - \frac{dX_s}{dt}\right) + K_b(X_b - X_s)$$

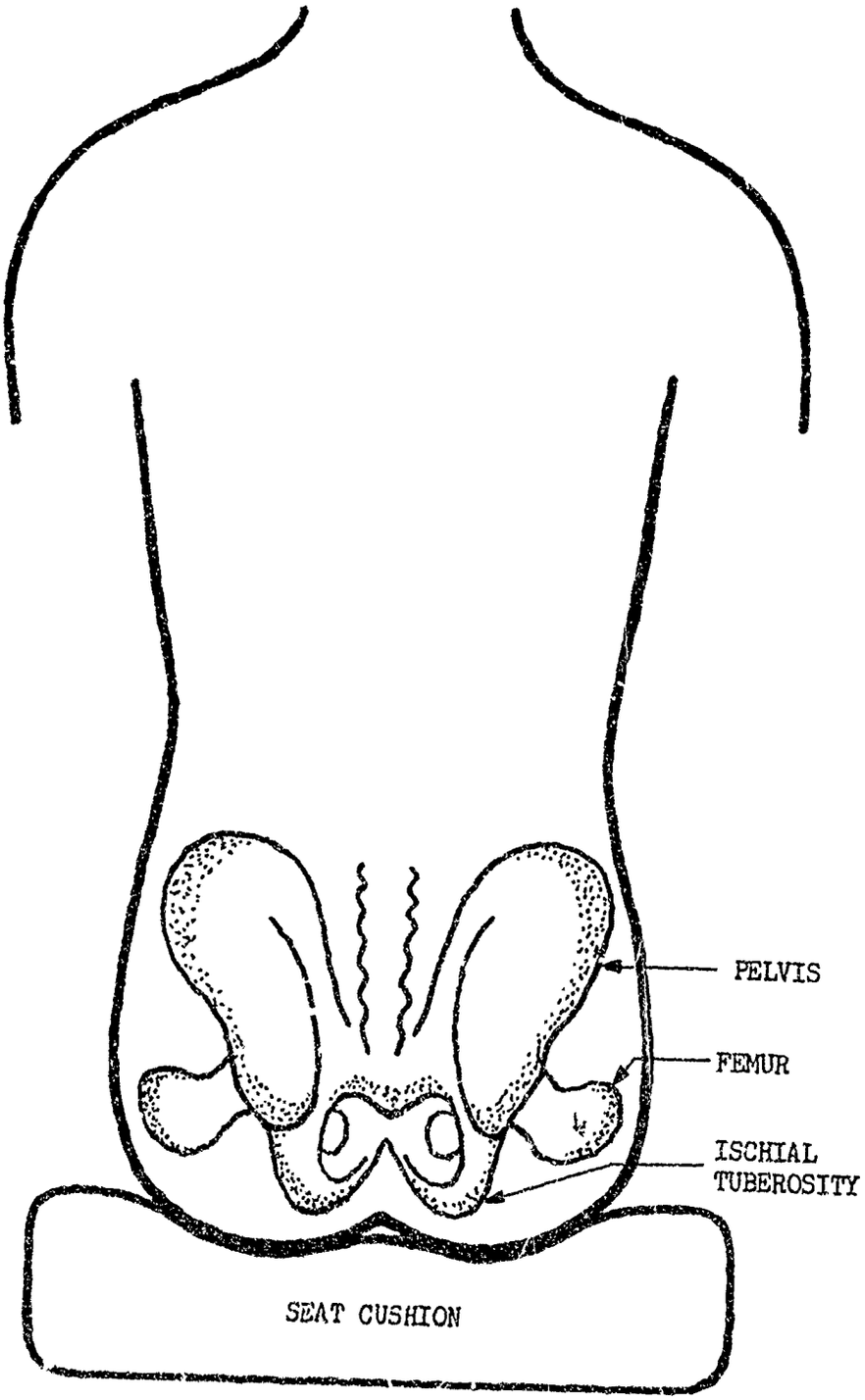


Figure 17. Body/Seat Diagram

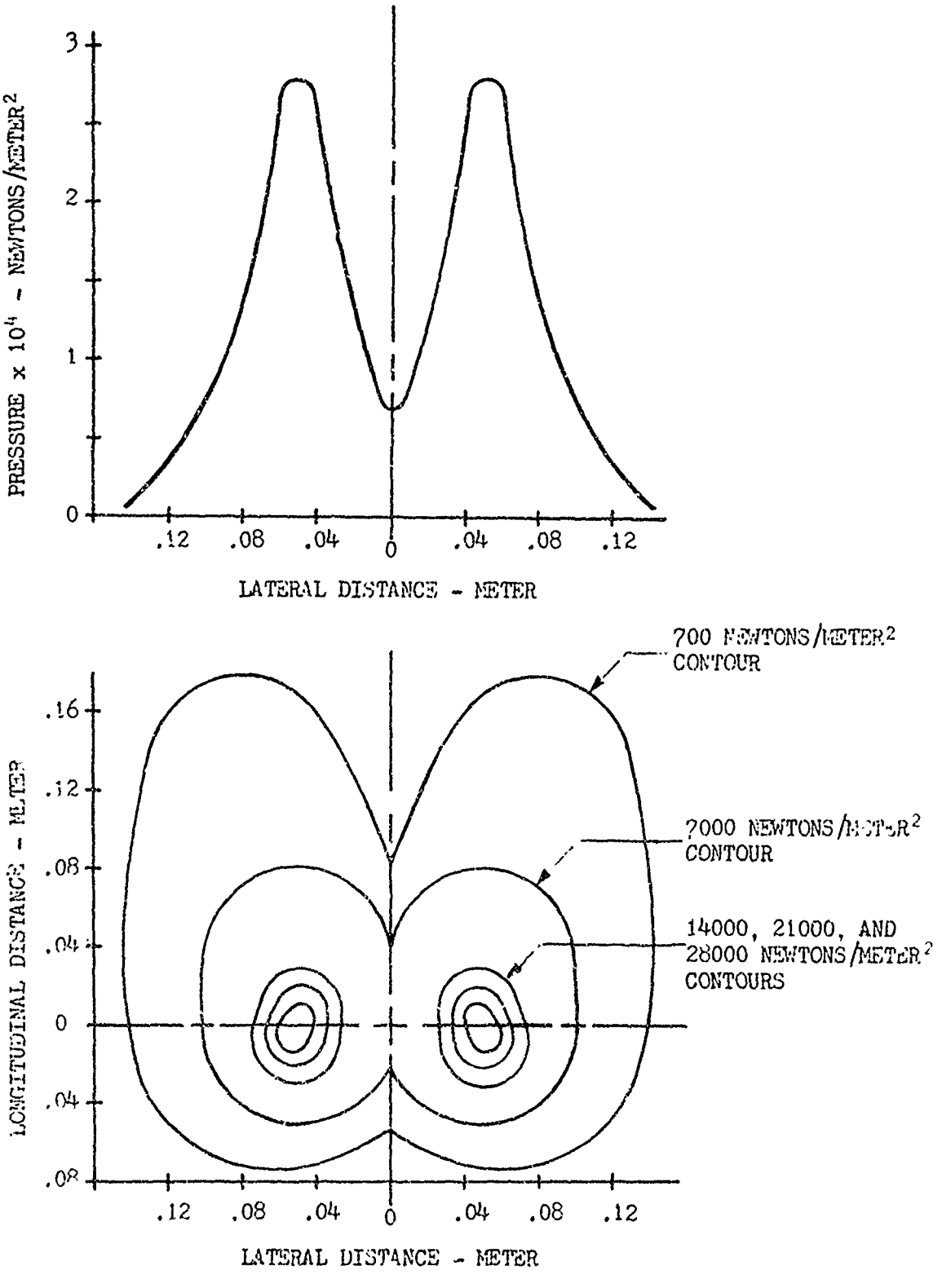


Figure 18. Approximate Buttocks Area Pressure Distribution (Redrawn from Hertzberg, 1955)

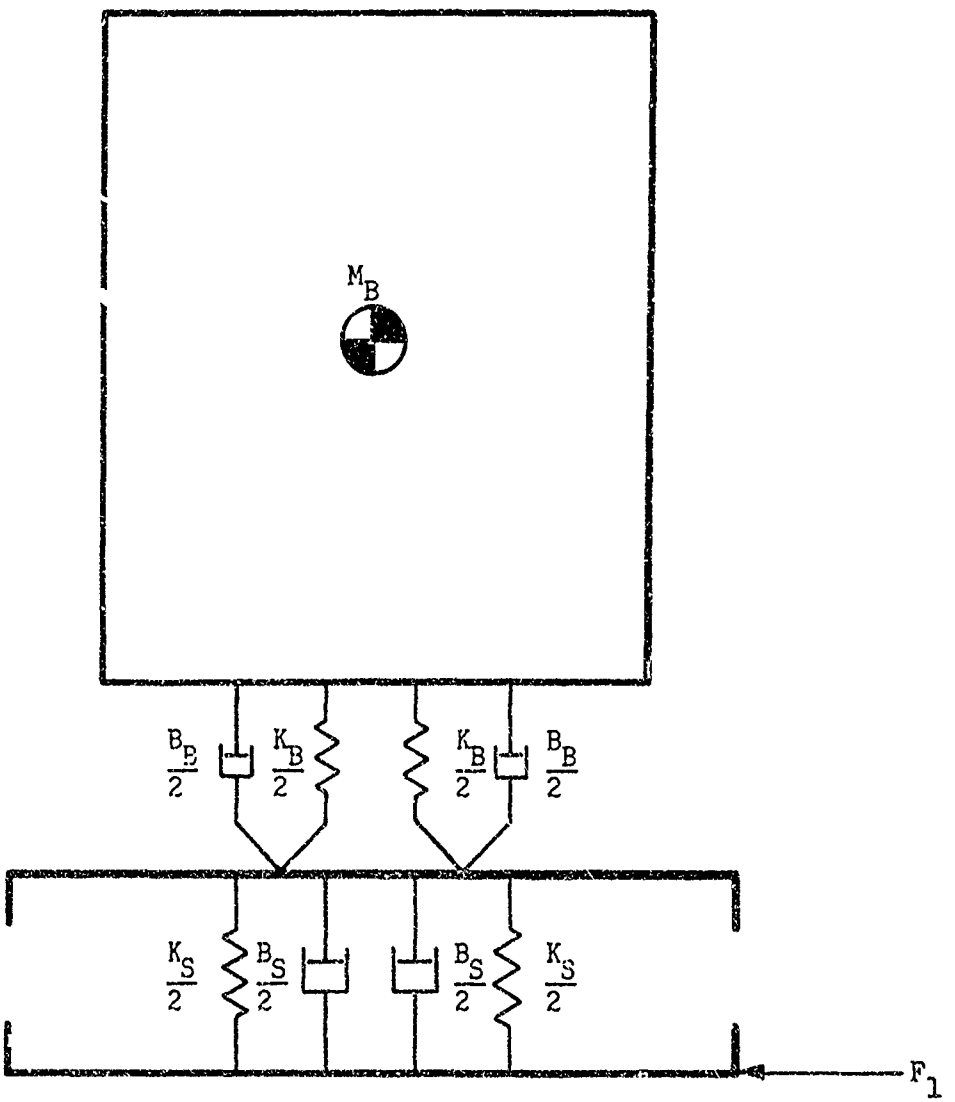


Figure 19. Body/Buttocks/Seat Model

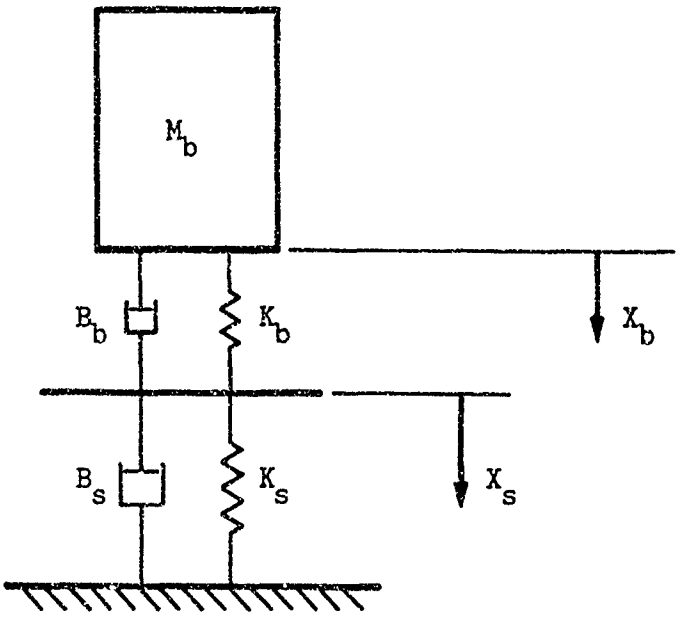


Figure 20. One-half Body/Buttocks/Seat Model

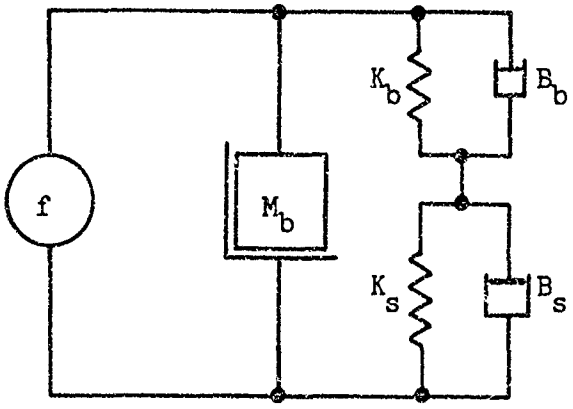


Figure 21. Mechanical Circuit Diagram

$$0 = -K_b(X_b - X_s) + K_s X_s - B_b \left(\frac{dX_b}{dt} - \frac{dX_s}{dt}\right) + B_s \frac{dX_s}{dt}$$

where: $M_b$ is one-half the mass of the body on the seat,

$K_b$ is the body flesh spring constant,

$B_b$ is the body flesh damping constant,

$X_b$ is the body skeletal displacement,

$K_s$ is the seat cushion spring constant,

$B_s$ is the seat cushion damping constant, and

$X_s$ is the seat displacement.

The following values were used in the implemented model:

$M_b$ = 28 kilograms,

$K_b$ = $3.17 \times 10^4$ newtons/meter,

$B_b$ = 840 newton seconds/meter,

$K_s$ = $1.21 \times 10^4$ newtons/meter, and

$B_s$ = 1680 newton seconds/meter.

The values for $K_b$ and $K_s$ were taken from experimental data taken on a single human subject and a typical seat cushion. These data are shown in Figures 22 and 23, respectively. The particular values for $K_b$ and $K_s$ were the linearized values over a range of body weight of from 340 to 780 newtons. This range of linearization was adequate for the model being stimulated by lateral forces. A lateral force shifts the body mass from side to side causing a change in force applied to the tuberosity areas through a change in mass applied. The values for $B_b$ and $B_s$ were determined through experimentation with the computer-implemented model and selected to make the model match observed subject/seat combination performance.

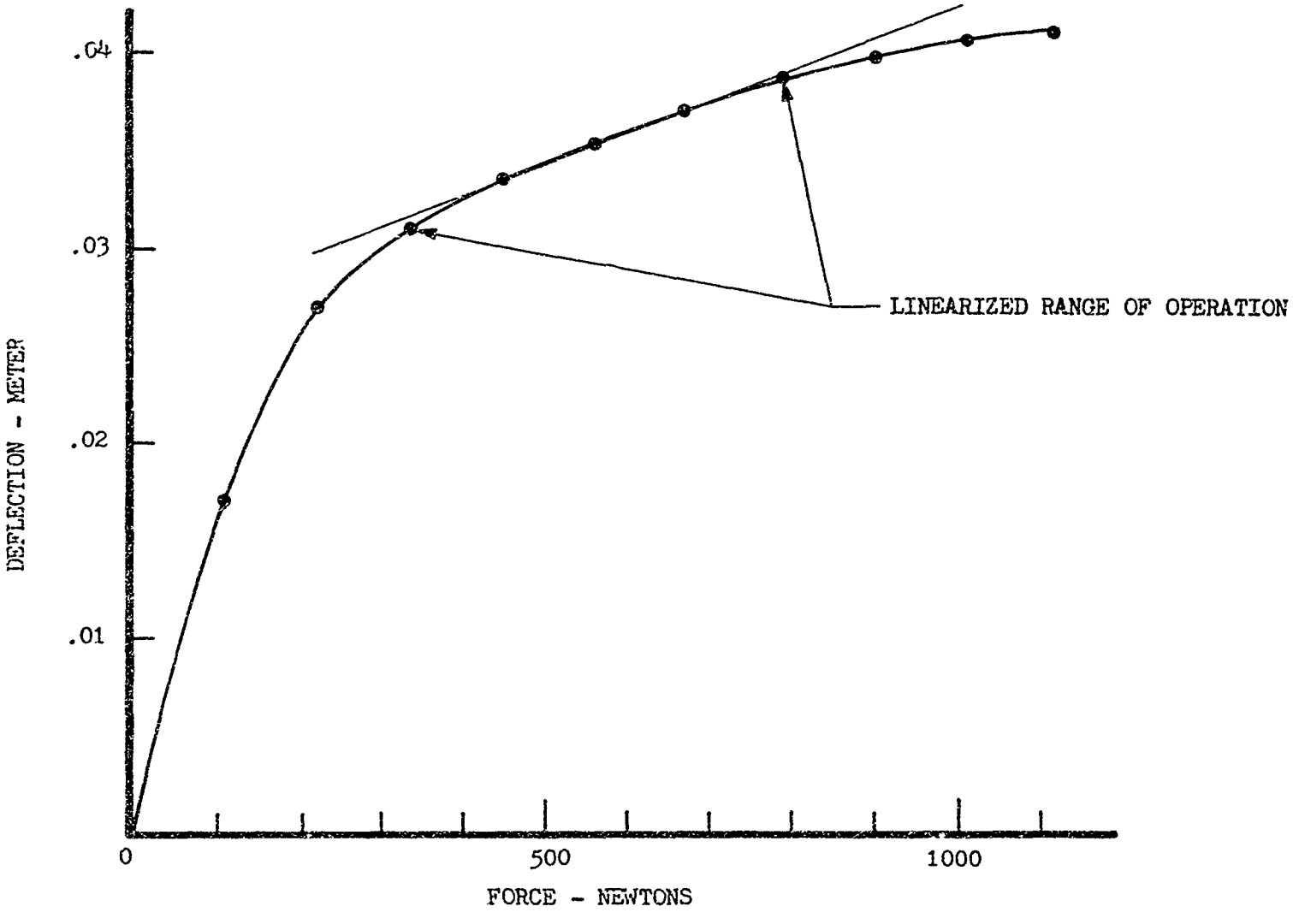


Figure 22. Deflection of Body Tissue under the Tuberosities As a Function of Applied Force

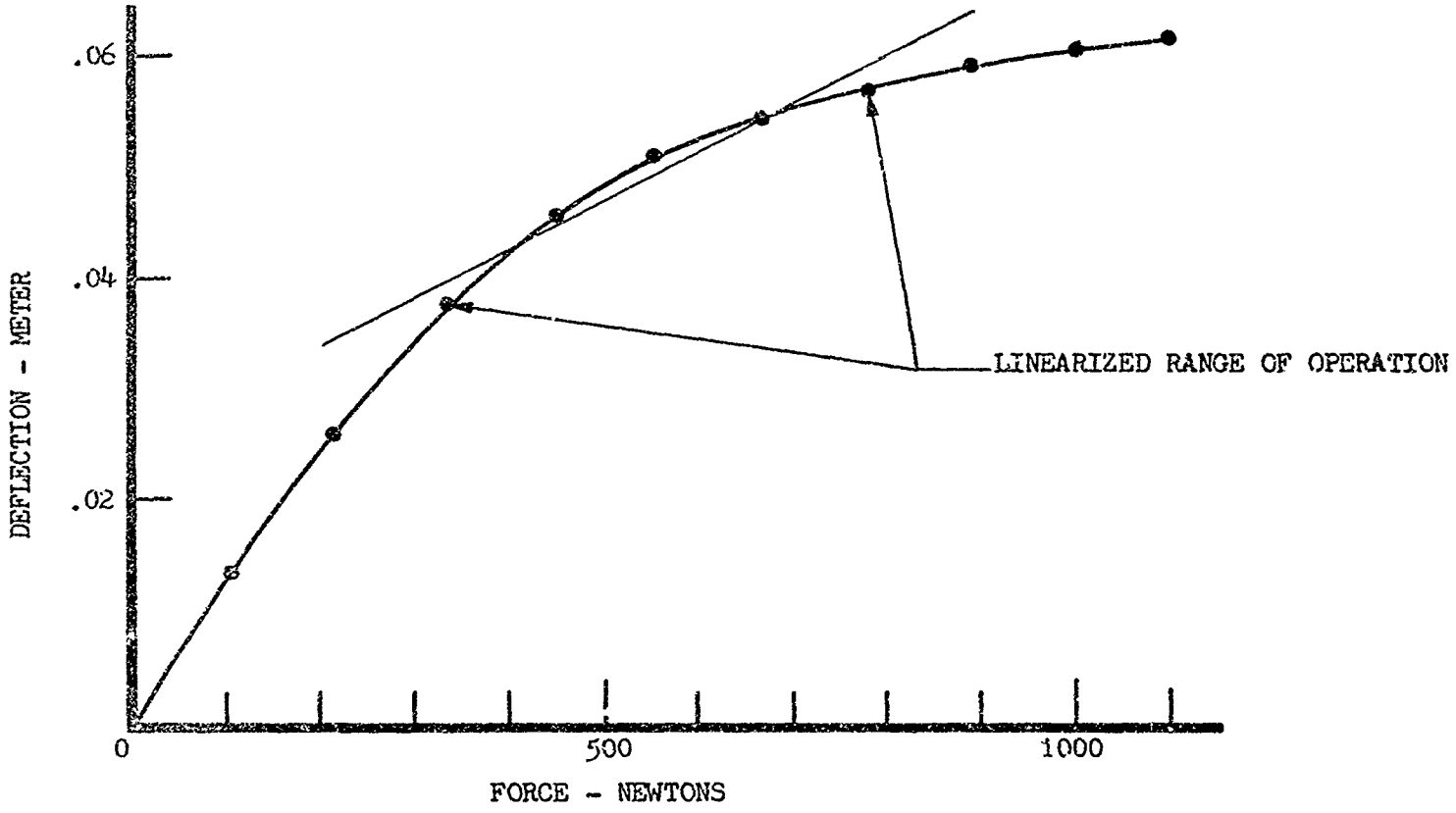


Figure 23. Deflection of Seat Cushion As a Function of Applied Force

Data were also taken for the buttocks area for contact area as a function of force applied to the buttocks, as shown in Figure 24. These data were not necessary for the body/buttocks/seat modeling, but were of interest from the standpoint of tactile receptor stimulation. However the tactile reception mechanism was not modeled.

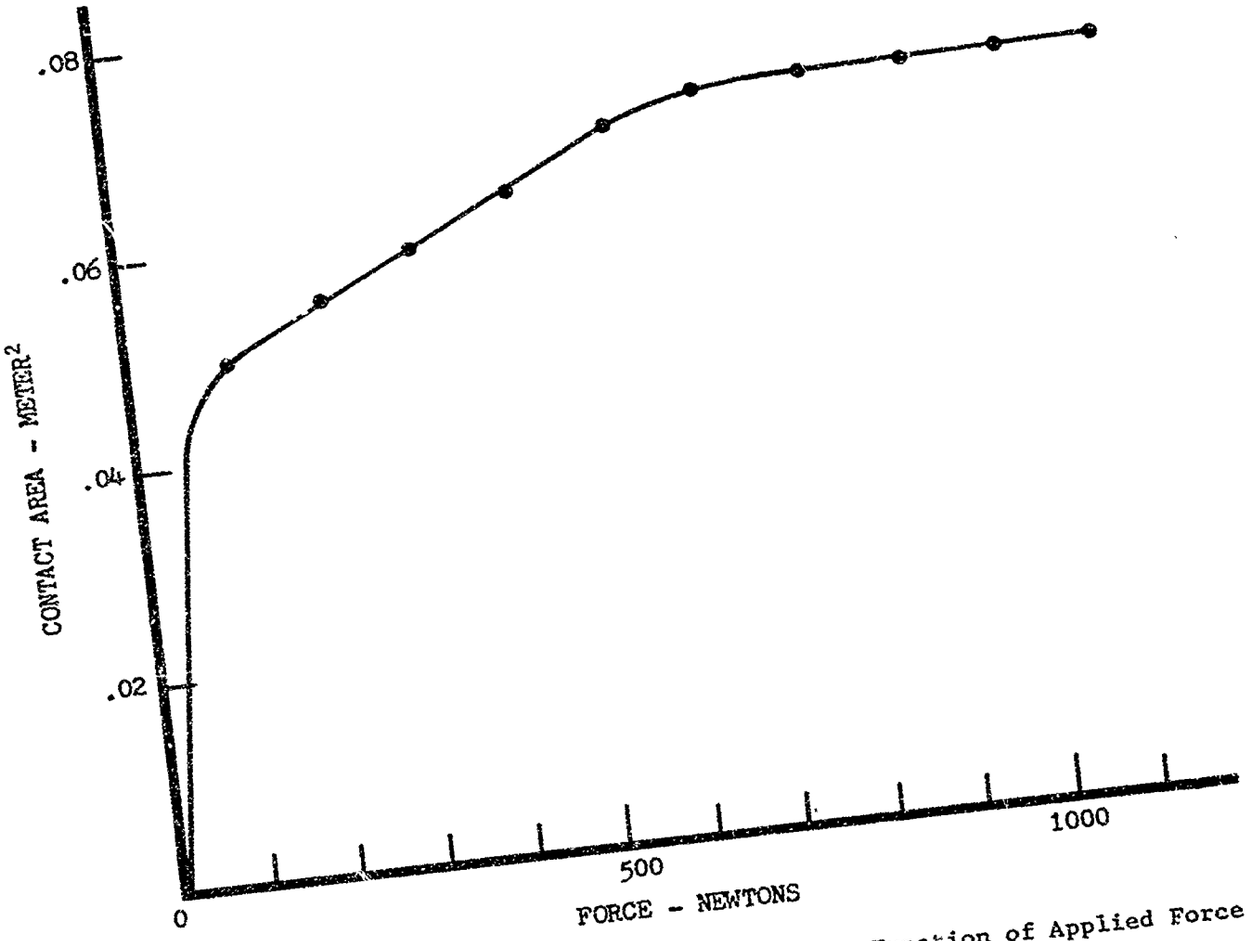


Figure 24. Buttocks Contact Area As a Function of Applied Force

## SECTION III
## MODEL PERFORMANCE

The performance of the four models--the semicircular canal, the otolith, the head/muscle, and the body pressure--was characterized by collecting various data on each. These data included: frequency response; response to step impulse and doublet acceleration inputs; and response to dynamic inputs typical of those received laterally by a pilot in an aircraft.

The gain and phase frequency response plots for the models are shown in Figures 25 through 29. Figure 25, taken from Young (Reference 2), is somewhat misleading in terms of representing the semicircular canal response for comparison with the response of the other models. It is the response of the canal model modified with an S added in the numerator of the canal dynamics transfer function so that velocity rather than acceleration can be used as the input signal. It represents the ratio of perceived angular velocity to input angular velocity. The other three models were tested with acceleration inputs; so for valid comparison, frequency response data for the unmodified canal model with an angular acceleration input were taken.

The upper end of the frequency response curves for the canal and otolith models have comparable responses for acceleration inputs, falling off beyond 0.1 hertz. The head/muscle and body pressure model frequency response curves start to fall off beyond about 2.0 hertz indicating that they are sensitive to higher frequencies in the range of those experienced in flight.

Figure 30 shows the semicircular canal cupula displacement and perceived angular velocity for a 5-second angular acceleration impulse input applied to the semicircular canal model. The slow decay of the

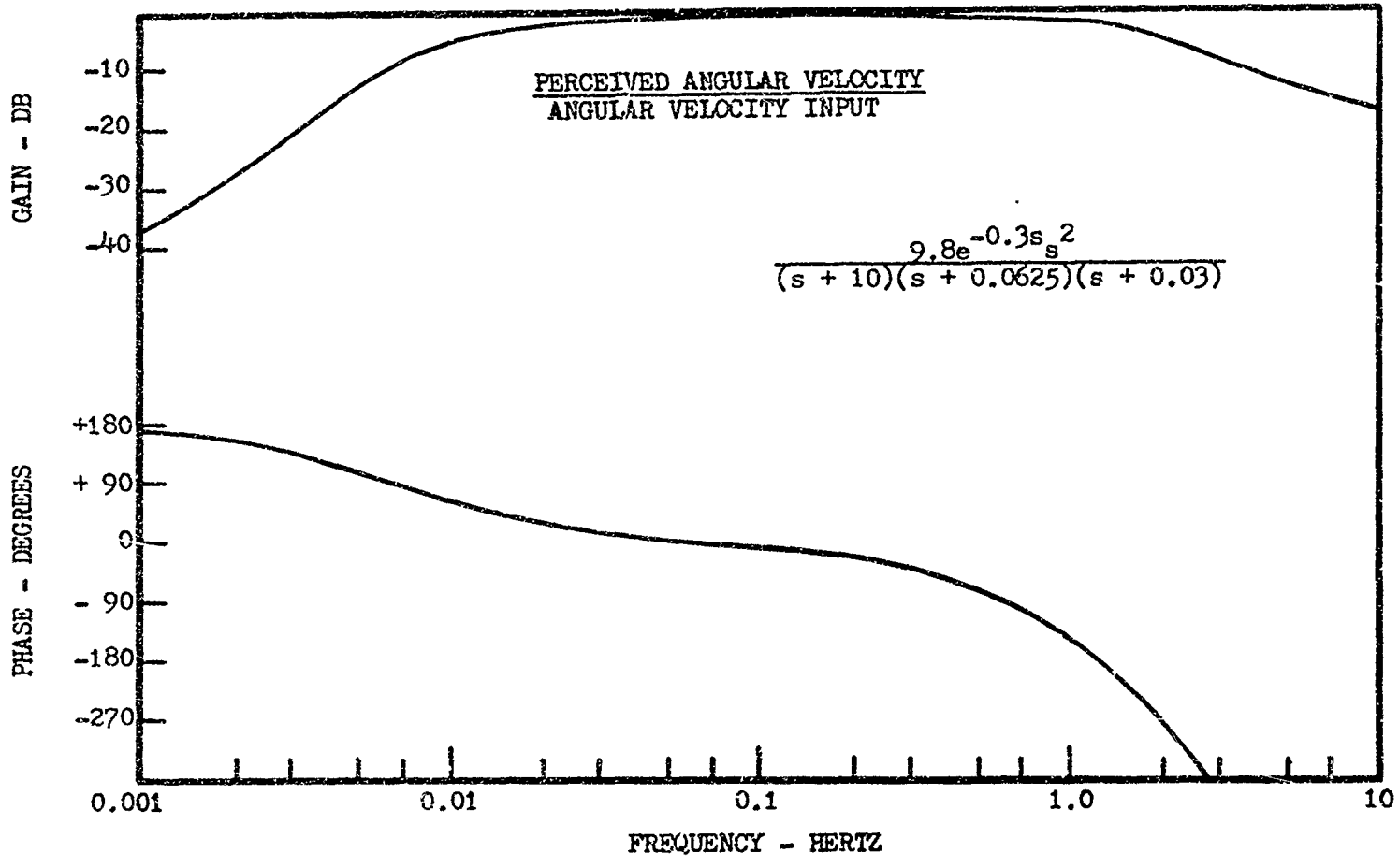


Figure 25. Semicircular Canal Model Frequency Response
(From Young et al., 1969)

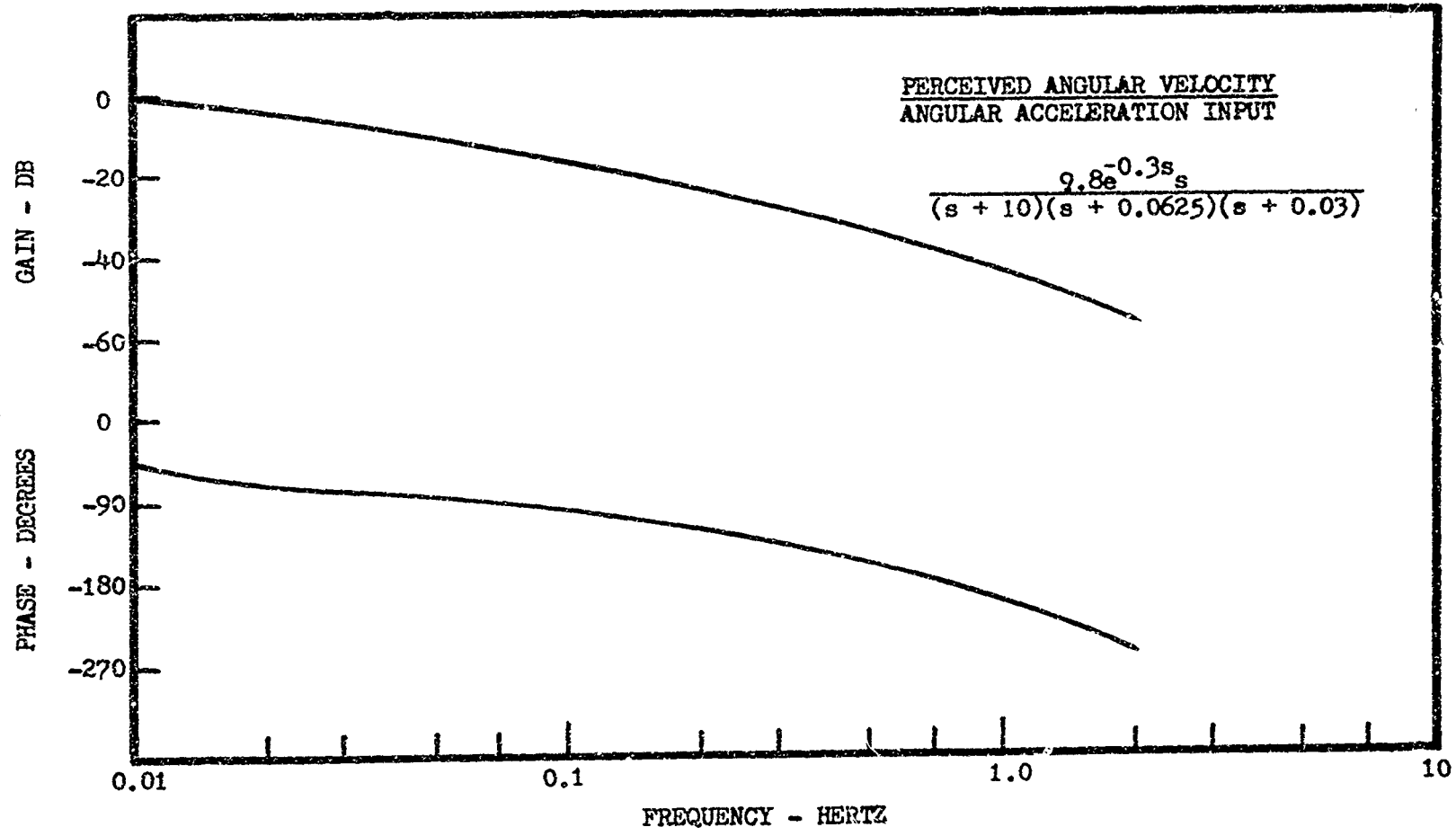


Figure 26. Semicircular Canal Model Frequency Response (Measured)

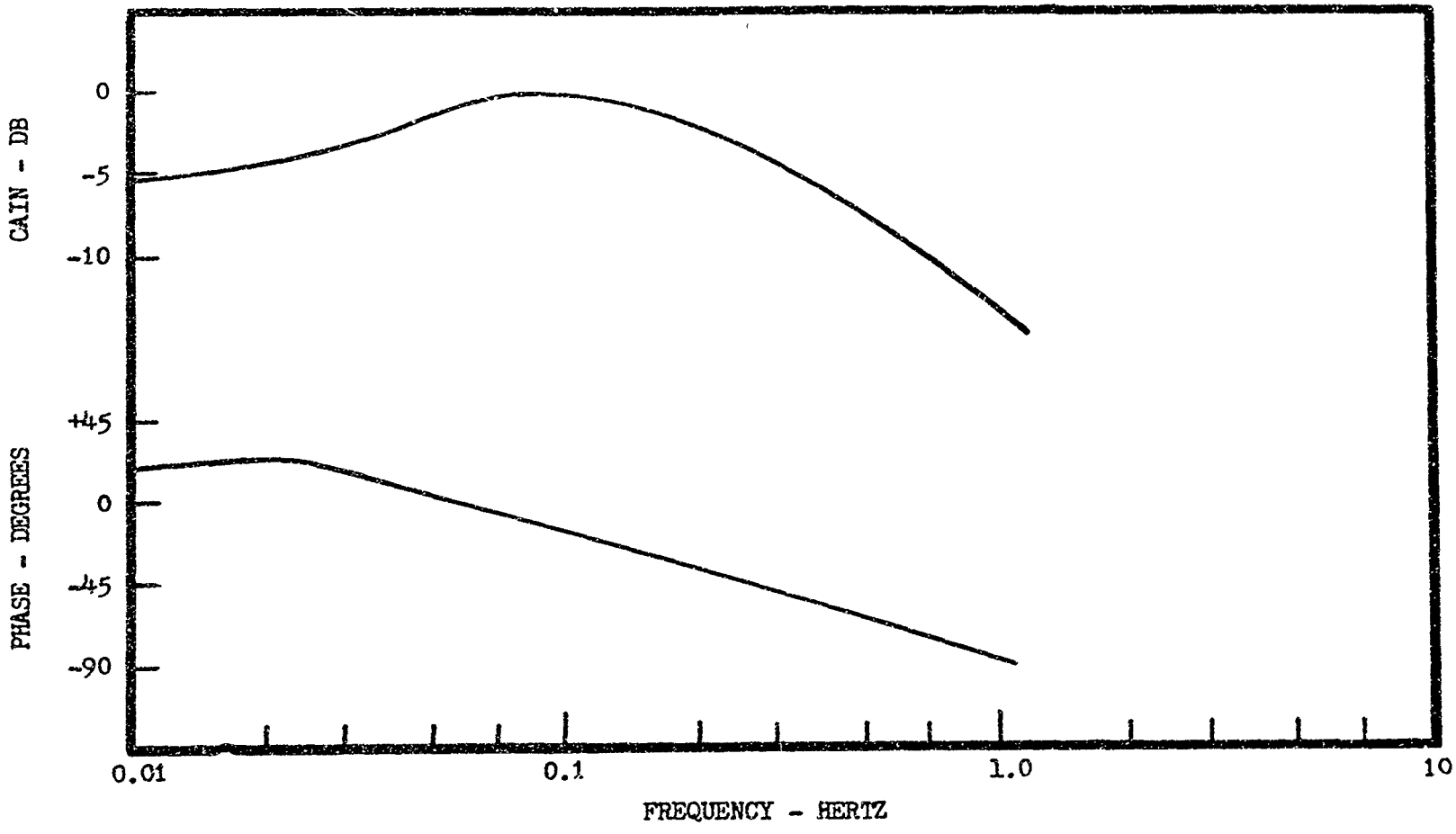


Figure 27. Otolith Model Frequency Response (From Young et al., 1969)

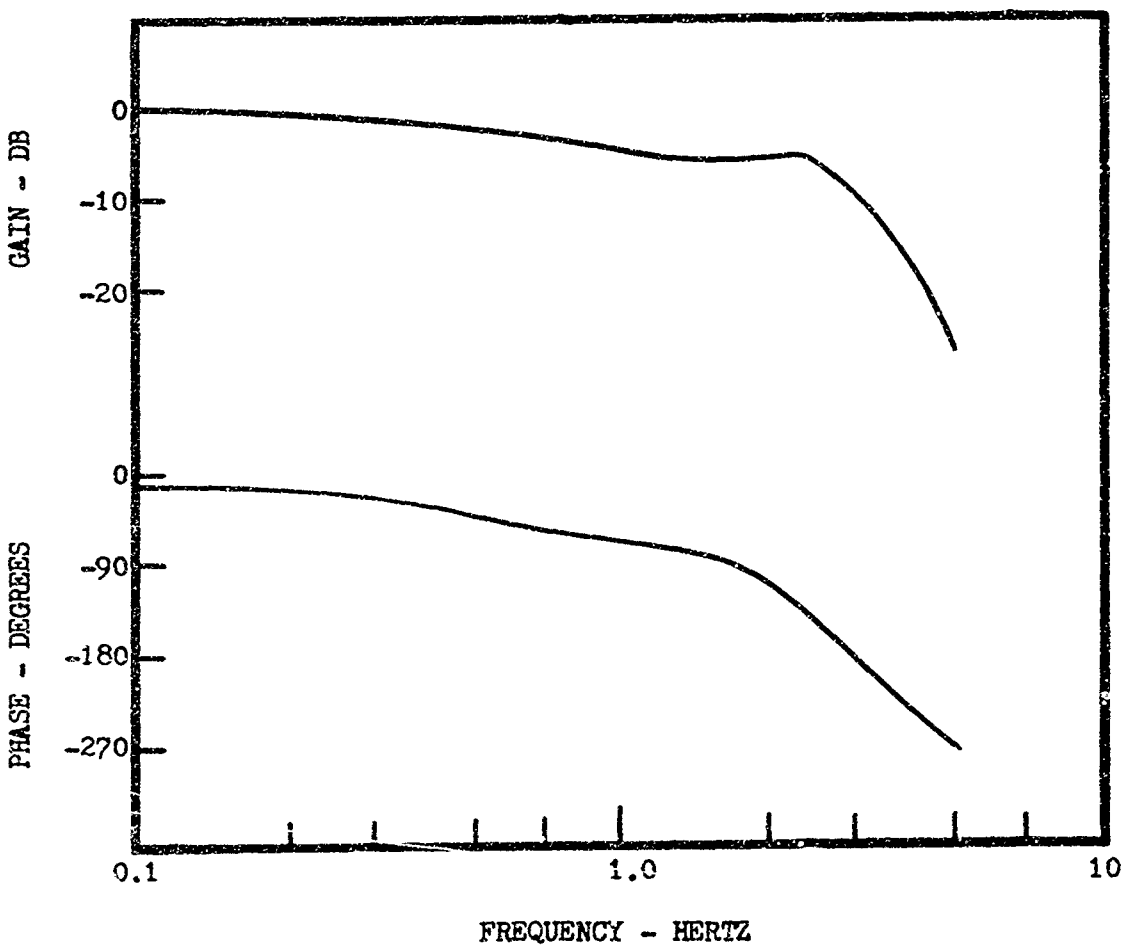


Figure 28. Head/Muscle Model Frequency Response

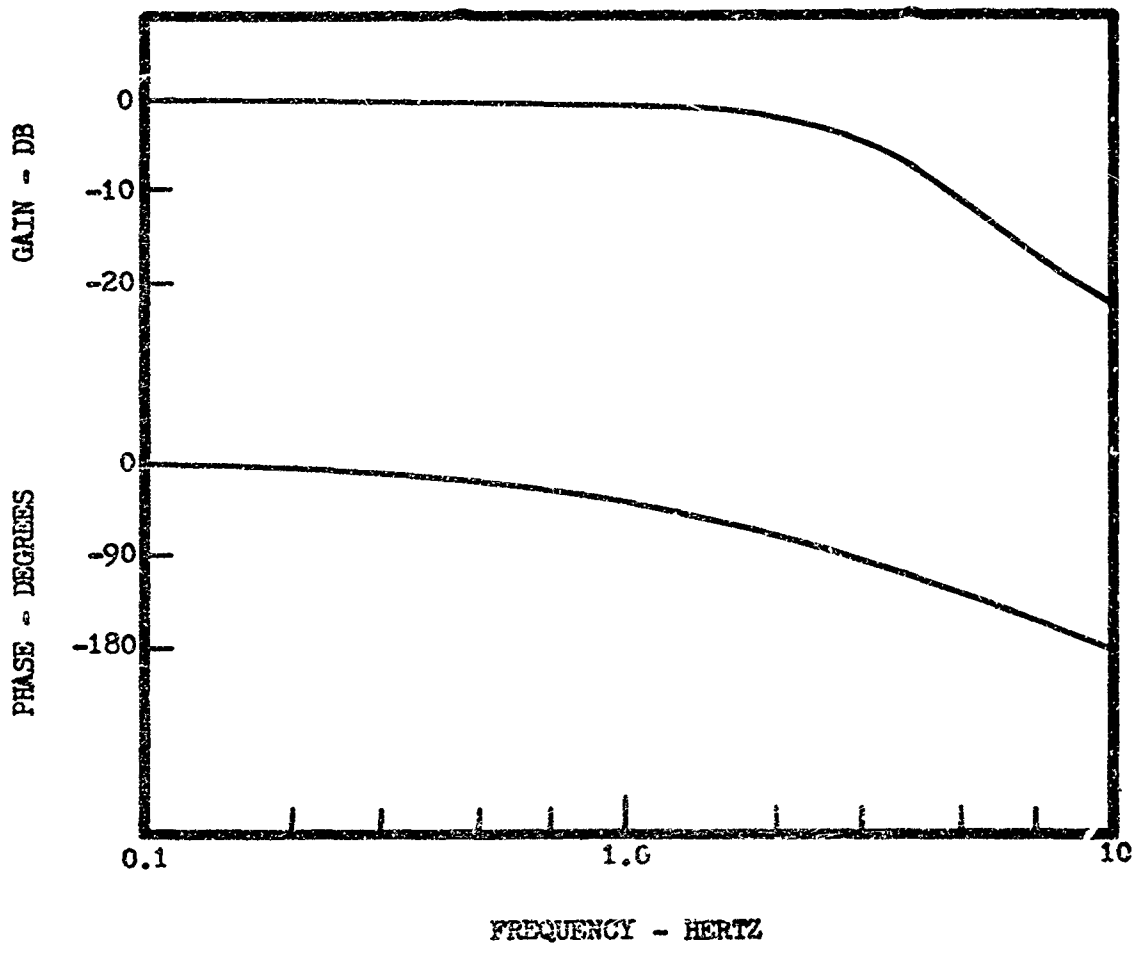


Figure 29. Body/Buttocks/Seat Model Frequency Response

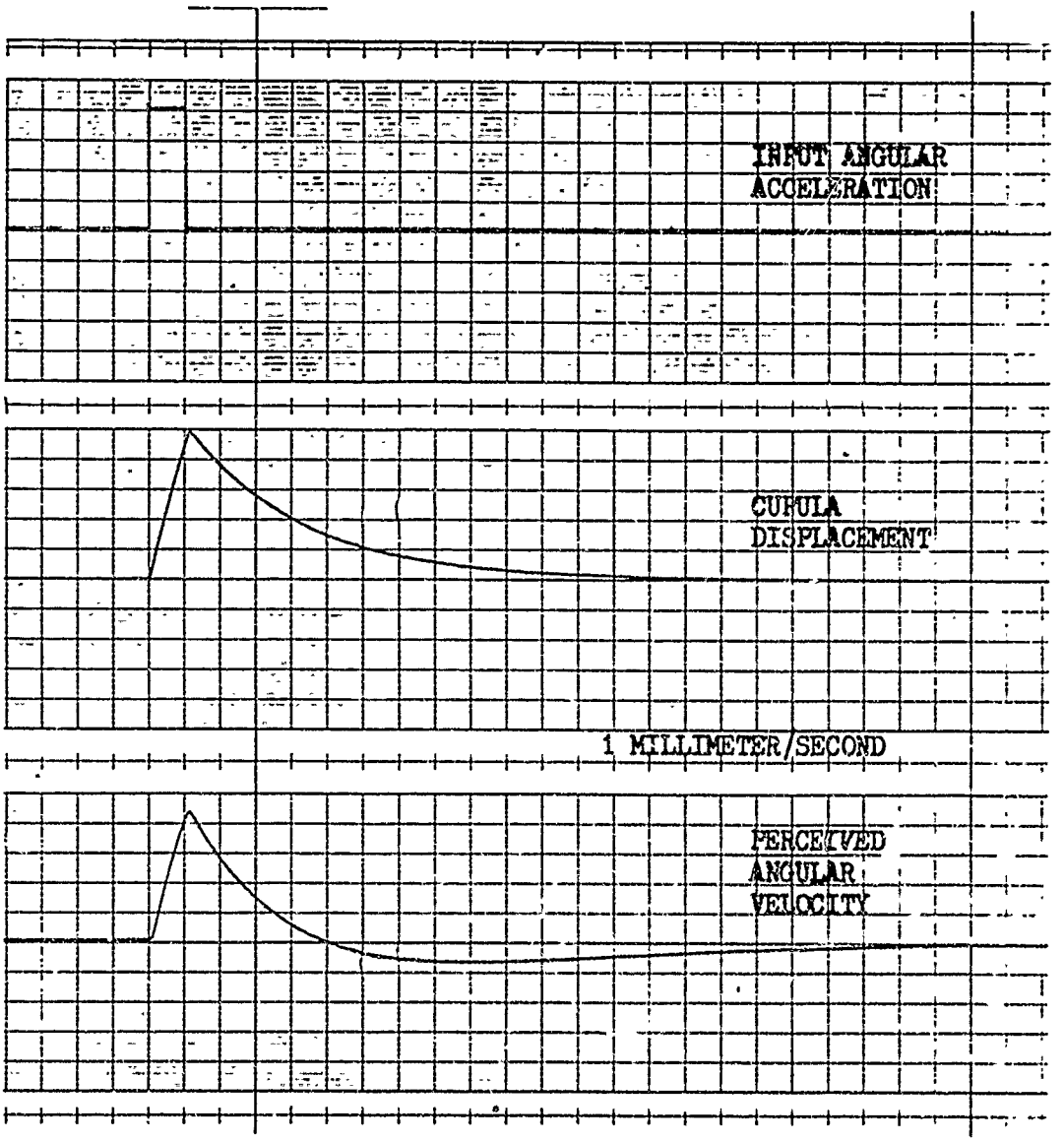


Figure 30. Semicircular Canal Model Response
To a 5-second Impulse

cupula displacement and perceived angular velocity is due to the fact that the input acceleration is removed before the canal system reaches a steady-state condition. The perceived angular velocity plot shows that a negative angular velocity is perceived about 25 seconds after the positive impulse input ends. This is due to the adaptation phenomenon. Figure 31 shows the responses for a 10-second angular acceleration doublet input. The semicircular canal for this forcing function perceives a negative angular velocity disproportionately larger for the negative cupula displacement due to the adaptation phenomenon.

Figure 32 shows the otolith displacement and perceived acceleration for a 25-second linear acceleration impulse input applied to the otolith model. The magnitude of the perceived acceleration decays with time to a fixed level for a sustained input due to the neural processing which produces a perceived acceleration based on otolith velocity as well as otolith displacement. When this sustained input is removed, the removal is sensed as a slight negative acceleration. Figure 33 shows the response for a 40-second linear acceleration doublet input. The simultaneous removal of a positive acceleration and application of an equal negative acceleration generates an enhanced perceived negative acceleration. This action is due to the neural processing part of the model which enhances the otolith sensitivity to changes in acceleration.

Figure 34 shows the angular displacement of the head and the muscle spindle feedback for various control position inputs applied to the head/muscle model. In this mode of operation the head/muscle system is acting as a position servomechanism responding to voluntary head movements. Figure 35 shows the angular displacement of the head and the muscle spindle feedback for various angular acceleration or torque disturbance inputs. Such torque could be applied to the head/muscle system through a lateral displacement of the body. As shown, there is little delay between the input torque and the muscle spindle

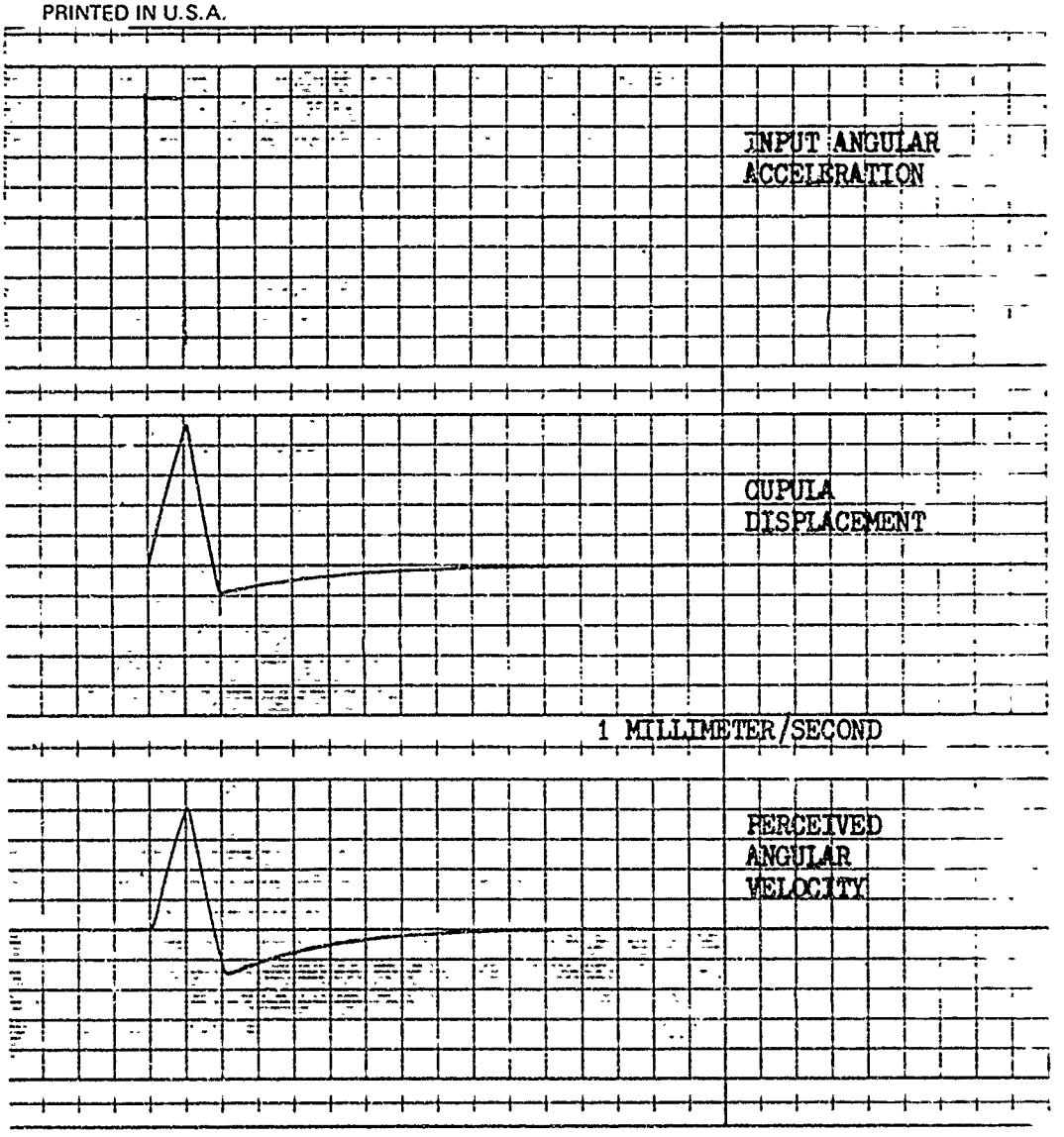


Figure 31. Semicircular Canal Model Response to a 10-second Doublet Impulse

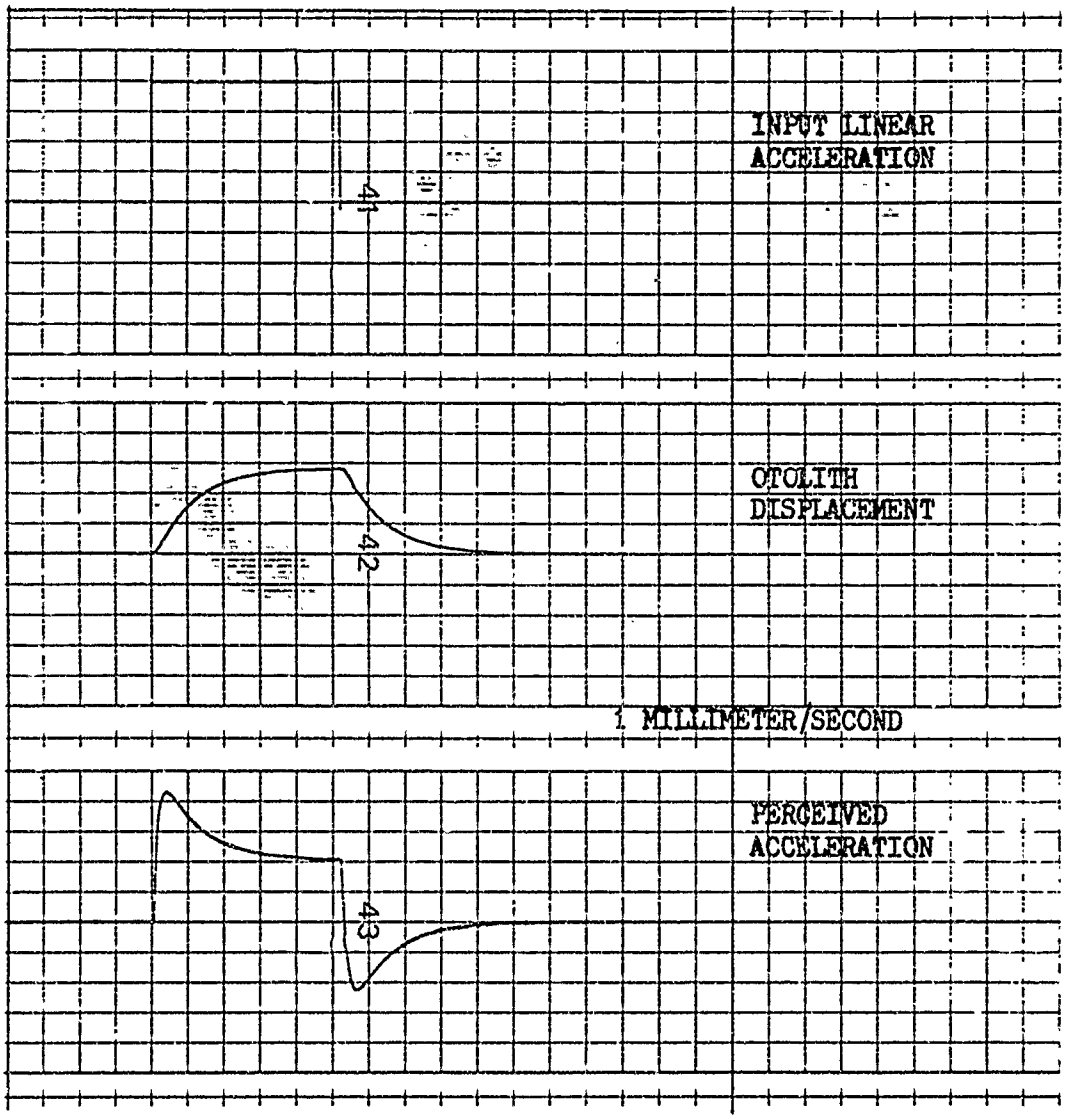


Figure 32. Otolith Model Response to a 25-second Impulse

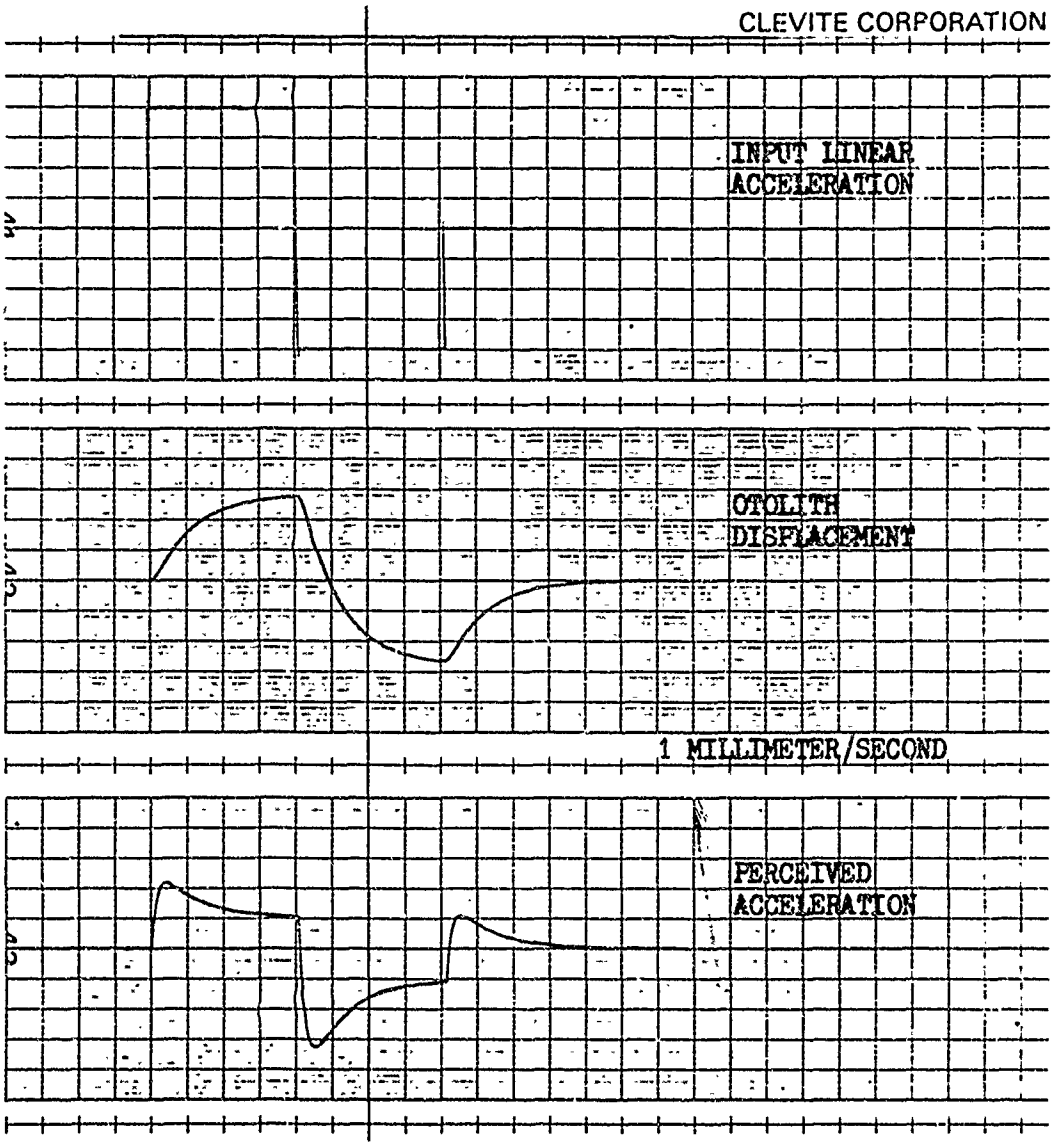


Figure 33. Otolith Model Response to a 40-second Doublet Impulse

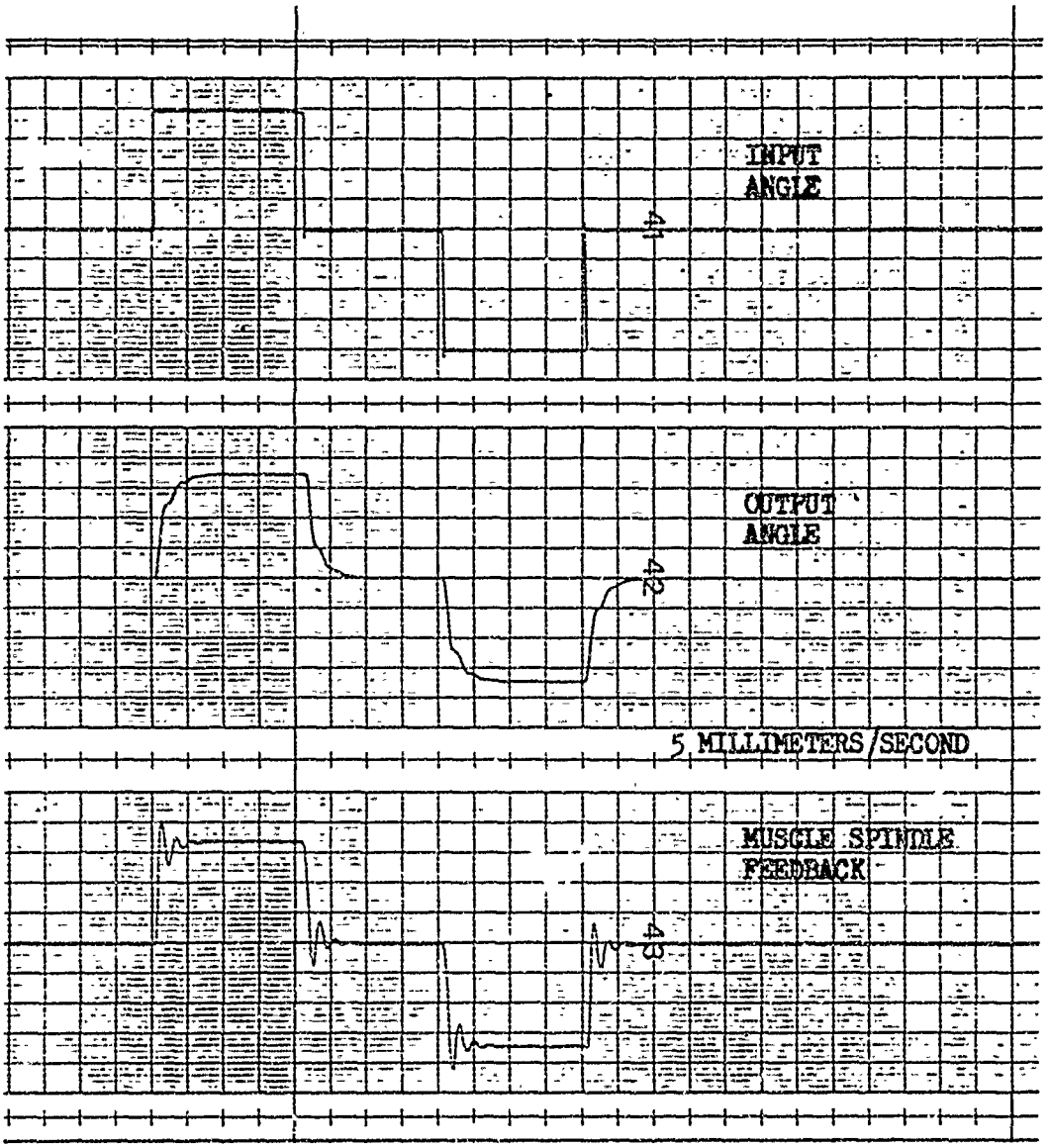


Figure 34. Head/Muscle Model Response to 4-second Impulses Applied to the Model Control Input

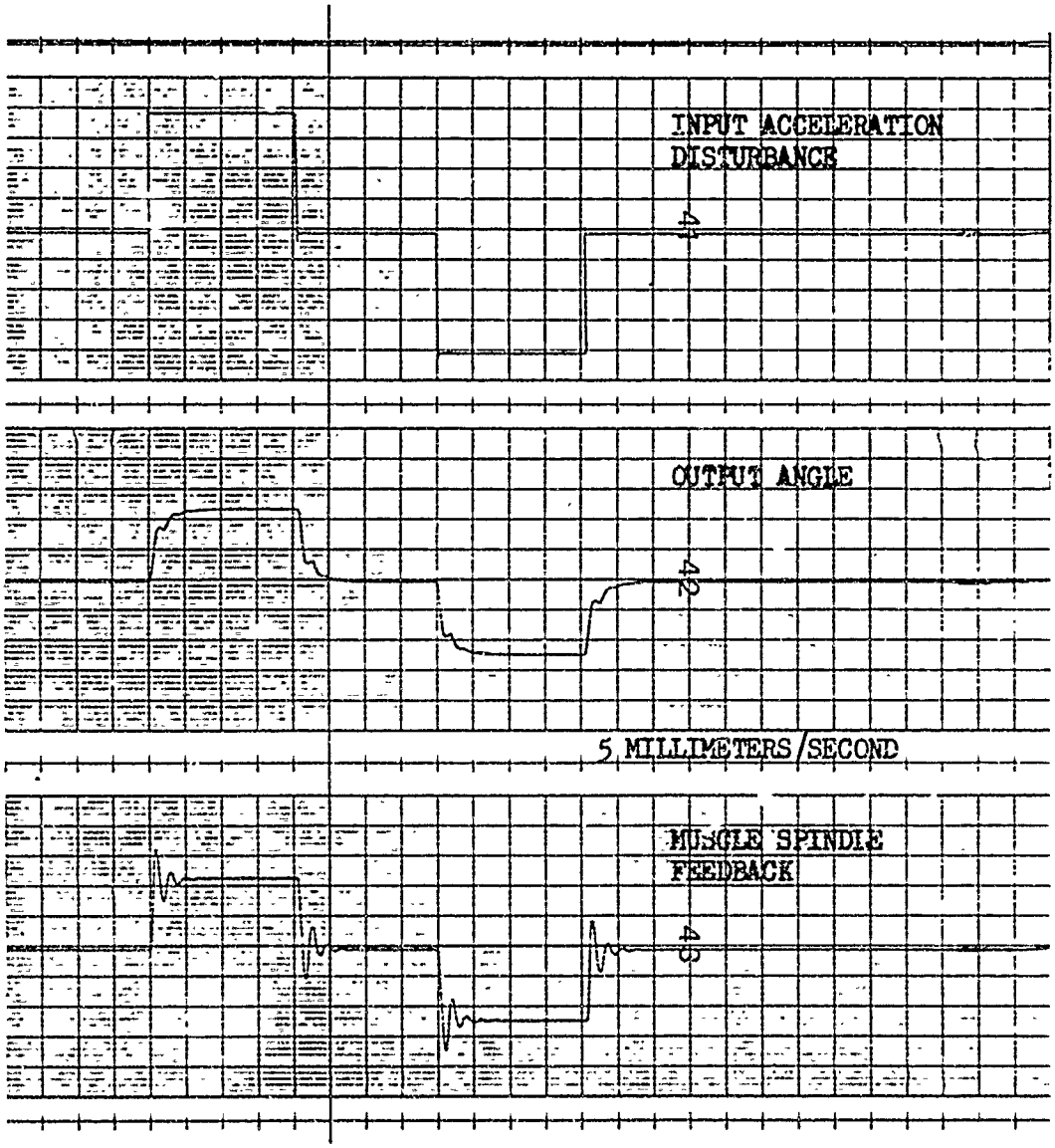


Figure 35. Head/Muscle Model Response to 4-second Impulses Applied to the Model Disturbance Input

feedback or torque sensing signal, indicating that this is a sensing mechanism that responds with little delay with a feedback signal very representative of the disturbance input.

Figure 36 shows the body skeletal vertical displacement, the aircraft seat displacement, and the buttocks compression for various forces applied to the body/buttocks/seat model. These vertical forces would result, considering lateral displacement excitation, from the body being shifted from side to side, thereby alternately increasing and decreasing the weight applied to the two tuberosity areas.

Figure 37 shows the buttocks compression and perceived pressure for an 8-second doublet input applied to the body pressure-sensing model. As shown, the buttocks compression closely follows the input force. However, the perceived pressure rapidly fades away due to the adaptation part of the model. The body pressure-sensing mechanism seems to respond with little delay and is sensitive, primarily to pressure changes.

Figure 38 shows the lateral aircraft dynamics used to excite the force and motion-sensing models. Shown is the rudder step input and the resulting sideslip angle, sideslip angular velocity, and sideslip angular acceleration. The frequency and damping closely resemble that of the short-period lateral dynamics of a fighter aircraft such as the F-100.

Figure 39 shows the response of the otolith and semicircular canal models excited by the appropriate lateral aircraft dynamics inputs. As shown, the otolith perceived acceleration lags the applied force by approximately 0.5 second. Also for an angular acceleration input to the semicircular canal model, the output or perceived angular velocity closely resembles the aircraft angular velocity, lagging by approximately 0.25 second. It must be kept in

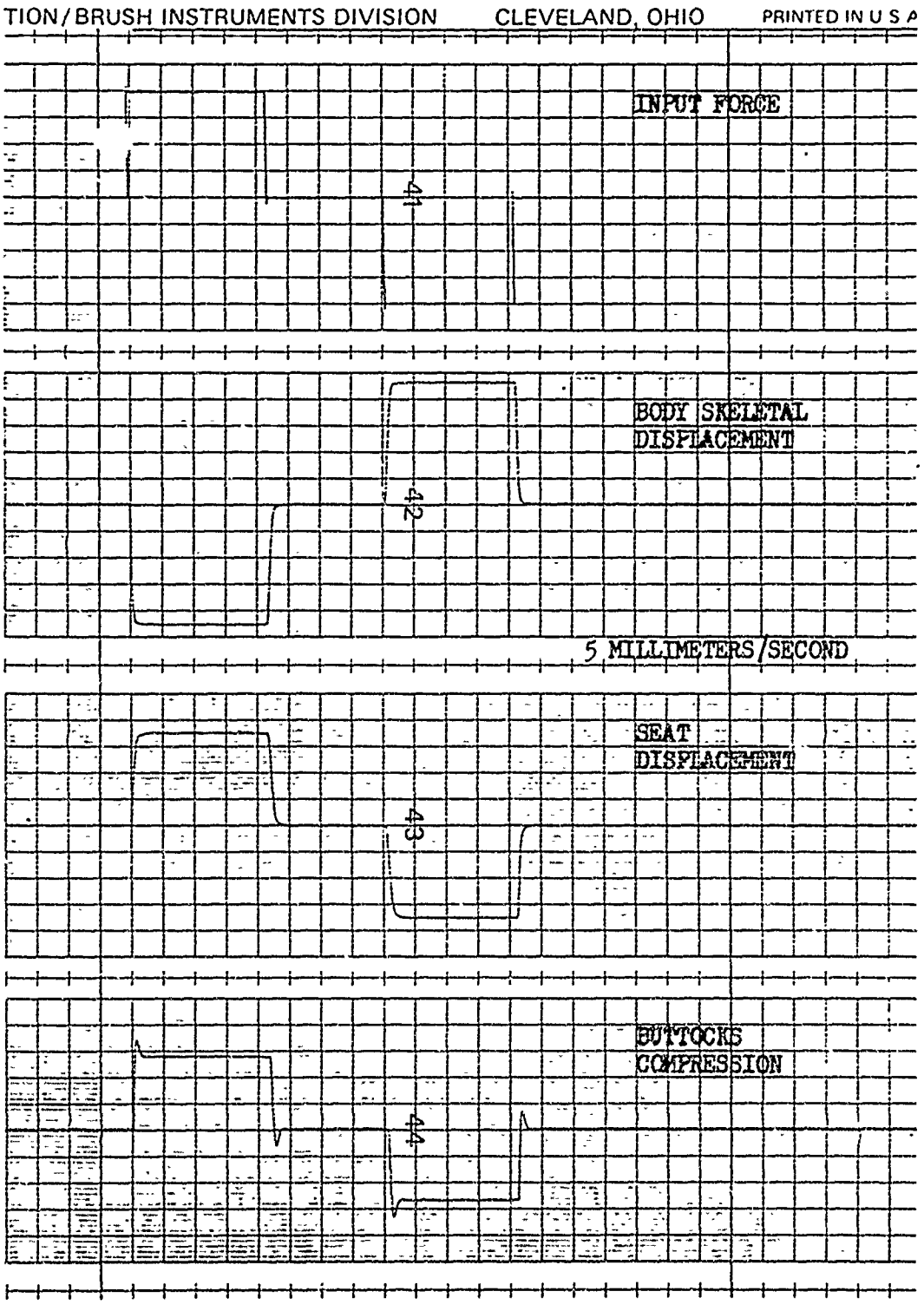


Figure 36. Body/Buttocks/Seat Model Response to 4-second Impulses

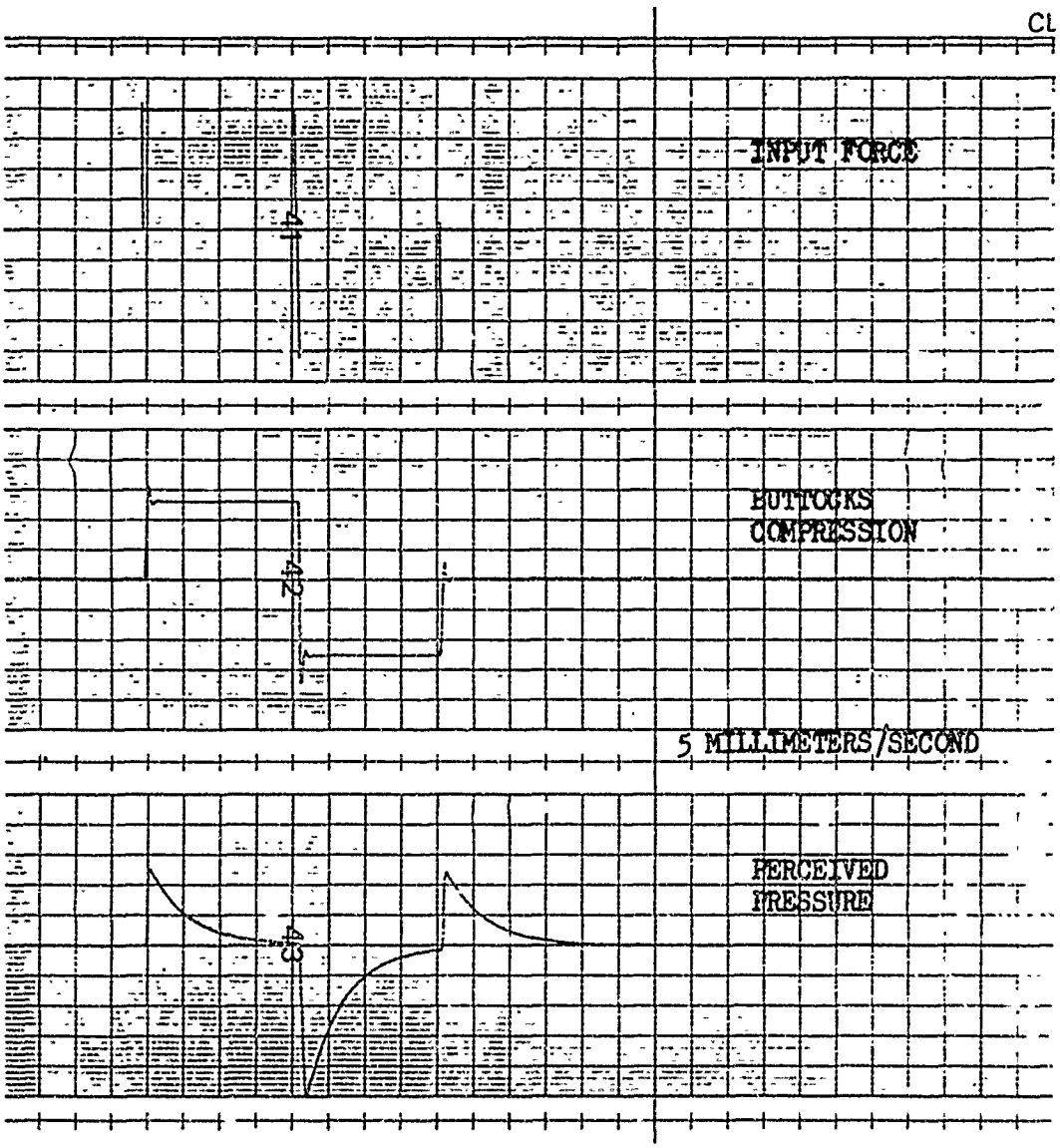


Figure 37. Body Pressure Sensing Model Response to an 8-second Doublet Impulse

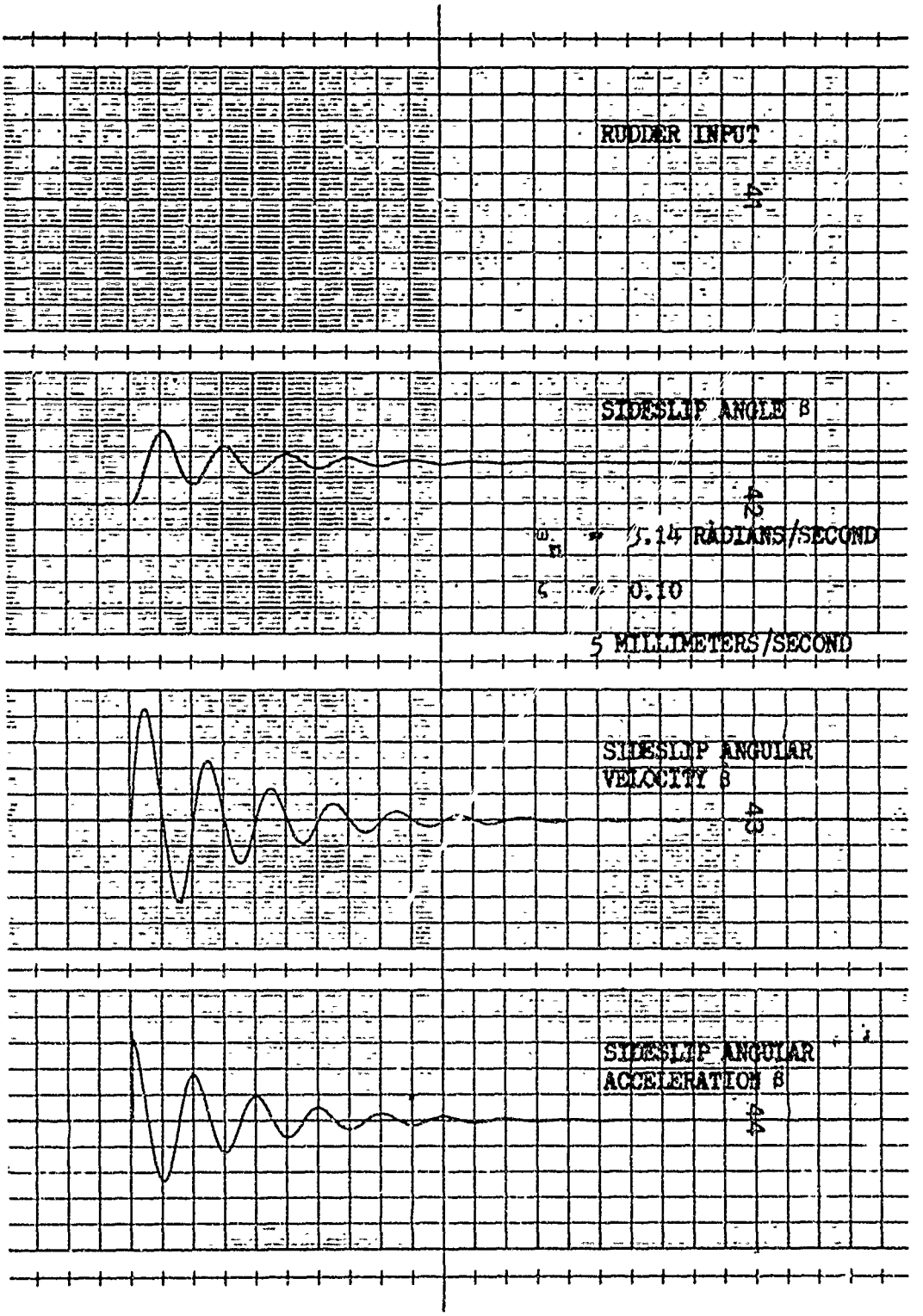


Figure 38. Lateral Aircraft Dynamics

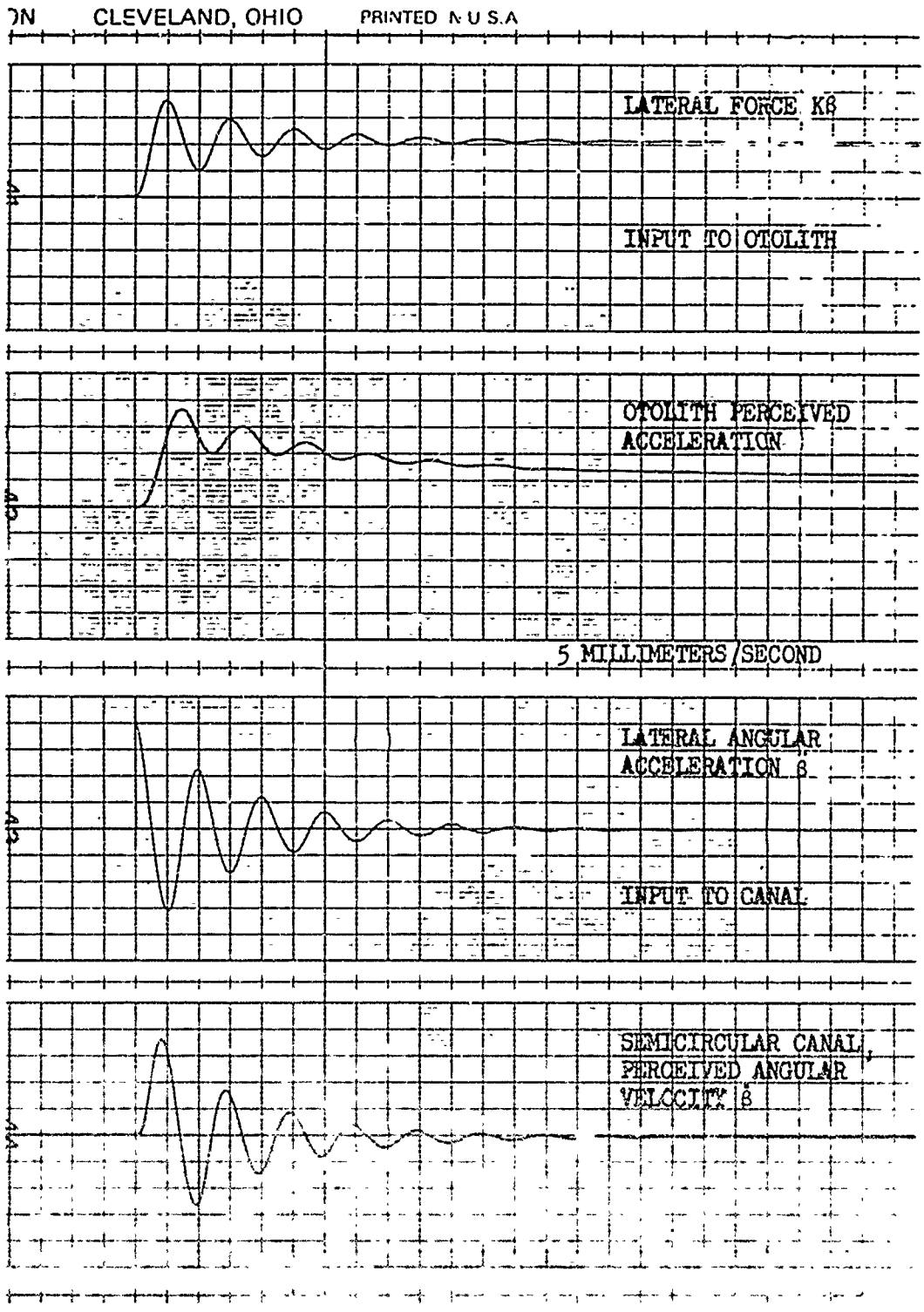


Figure 39. Otolith and Semicircular Canal Model Responses to Lateral Aircraft Dynamics Input

mind that the lateral aircraft dynamics as applied to the semicircular canals and otolith assume a rigid torso and an unmoving head with no motion relative to the aircraft.

Figure 40 shows the relative responses for the otolith, head/muscle, and body pressure models for a common lateral force. As shown, the head/muscle and body pressure models respond with very little delay.

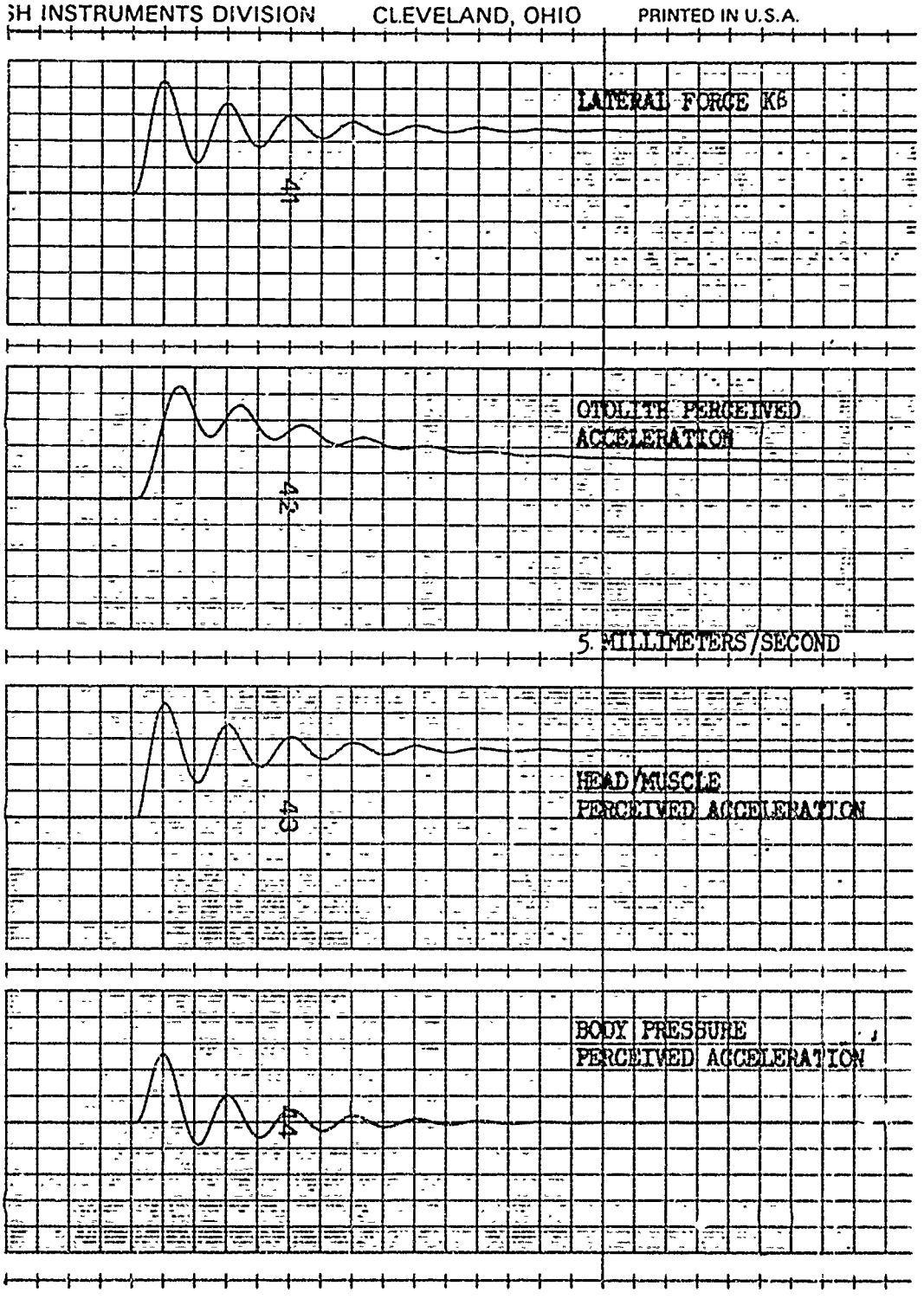


Figure 40. Otolith, Head/Muscle, and Pressure Model Responses to Lateral Aircraft Dynamics

## REFERENCES


1. Huston, Dr. Robert C., "American Airlines' Training Innovations," Simulation Symposium, 1972.

2. Young, L. R., Meiry, J. L., Newman, J. S., and Feather, J. E., "Research in Design and Development of a Functional Model of the Human Nonauditory Labyrinths," AMRL-TR-68-102, 1969.

3. Milsum, John H., Biological Control Systems Analysis, McGraw-Hill, New York, 1966.

4. Davson, H., and Eggleton, M. G., ed., Starling and Lovatt Evans Principles of Human Psysiology, 13th Edition, Lea and Febiger, Philadelphia, 1962.

5. Stark, L., Neurological Feedback Control Systems, Plenum Press, New York, 1966.

6. Buller, A. J., and Lewis, D. M., "The Rate of Tension Development in Isometric Tetanic Contractions of Mammalian Fast and Slow Skeletal Muscle," J. Physiol., Vol. 176, 1965.

7. Nashner, Lewis M., "Sensory Feedback in Human Posture Control," Sc. D. Thesis, M. I. T., 1970.

8. Clauser, C. E., McConville, J. T., and Young, J. W., "Weight, Volume, and Center of Mass of Segments of the Human Body," AMRL-TR-69-70, Aug. 1969.

9. Lippold, O., Nicholla, J., and Redfearn, J., "Electrical and Mechanical Factors in the Adaptation of a Mammalian Muscle Spindle," J. Physiol., Vol. 153, 1960.

10. Agarwal, G., Gottlieb, G., and Stark, L., "Models of Muscle Proprioceptive Receptors," Fourth Annual NASA-University Conference on Manual Control, NASA SP-192, 1968.

11. Grossman, Sebastian P., A Textbook of Physiological Psychology, John Wiley & Sons, Inc., New York, 1967.

12. Strughold, Hubertus, "The Mechanoreceptors of Skin and Muscles under Flying Conditions," German Aviation Medicine World War II, Vol. II, Department of the Air Force, April, 1950.

13. Swearingen, J. J., Wheelwright, C. D., and Garner, J. D., "An Analysis of Sitting Areas and Pressures of Man," Civil Aeromedical Research Institute, 62-1, FAA, Oklahoma City, Oklahoma, 1962.

14. Hertzberg, H. T. E., "Some Contributions of Applied Physical Anthropology to Human Engineering," Annals of the New York Academy of Sciences, Vol. 63, Art. 4, pp. 616-629, 1955.

15. Bennett, E., Degan, J., and Spiegel, J., ed., Human Factors in Technology, C. A. Dempsey, "The Design of Body Support and Restraint Systems," Chapt. 10, McGraw-Hill, New York, 1963.

16. Dempsey, Charles A., and Morrison, Lt. Nina K., Unpublished data on Buttocks Pressure Areas, 1955.

17. Milhorn, Howard T., Jr., The Application of Control Theory to Physiological Systems, W. B. Saunders, Philadelphia, 1966.

18. Christensen, K. K., and Johnson, L. L., "Study to Determine Methods of Simulating g Effects," WADC Technical Note 58-314, ASTIA 211849, Oct. 1958.

19. Hixson, W. C., Niven, J. I., and Correia, M. J., "Kinematics Nomenclature for Physiological Accelerations," Monograph 14, Naval Aerospace Medical Institute, NASA, Aug. 1966.

20. Borlace, Frank H., "Flight Simulator Motion, Its Enhancement and Potential for Flight Crew Training," SAE Third International Simulation and Training Conference, New York, 1967.

21. Kron, G. L., Unpublished Data on the Design of a Sustained "g" Seat for the Advanced Simulator for Undergraduate Pilot Training (ASUPT).

# APPENDIX A
# ANALOG COMPUTER DIAGRAMS

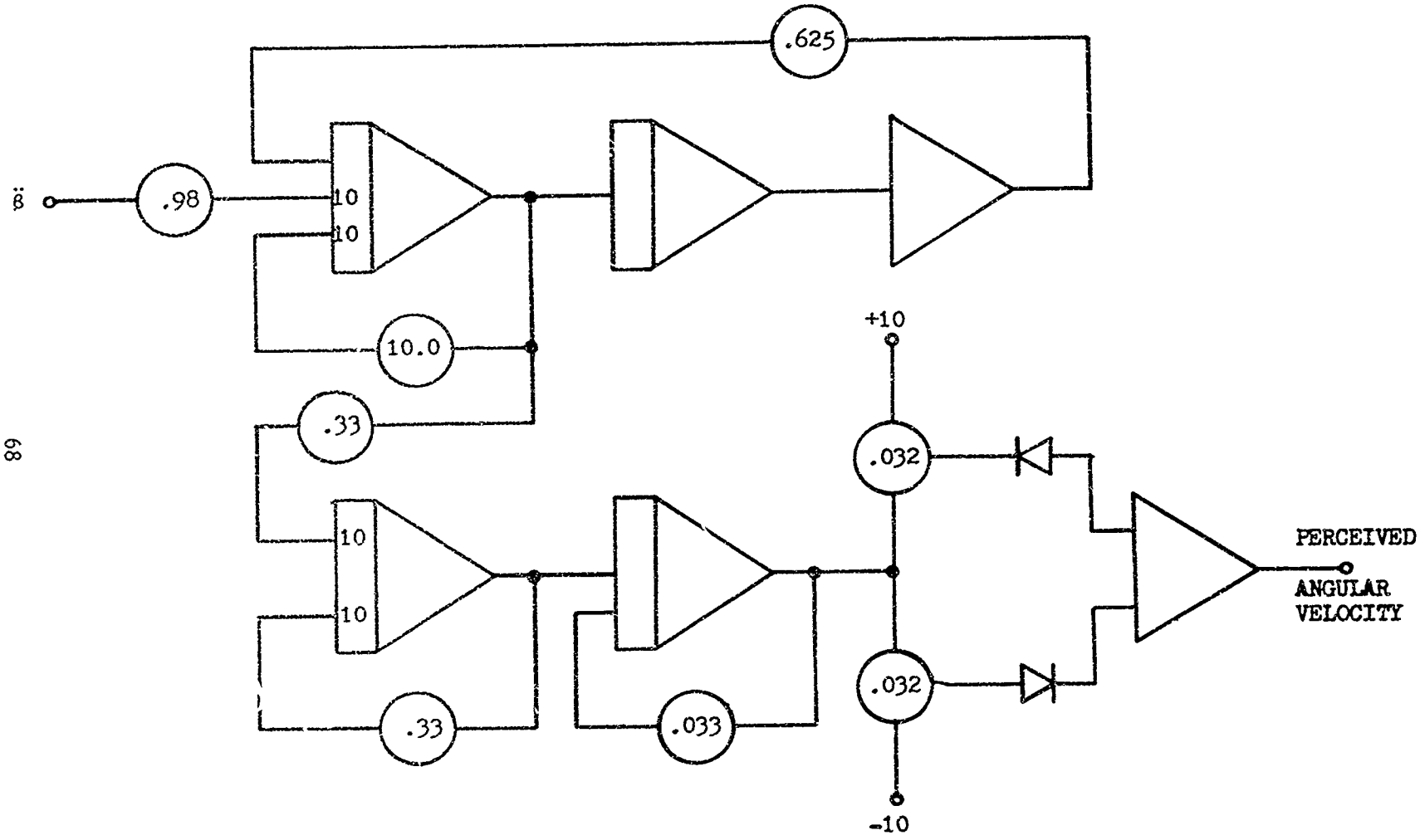


Figure 41. Semicircular Canal Model Computer Diagram

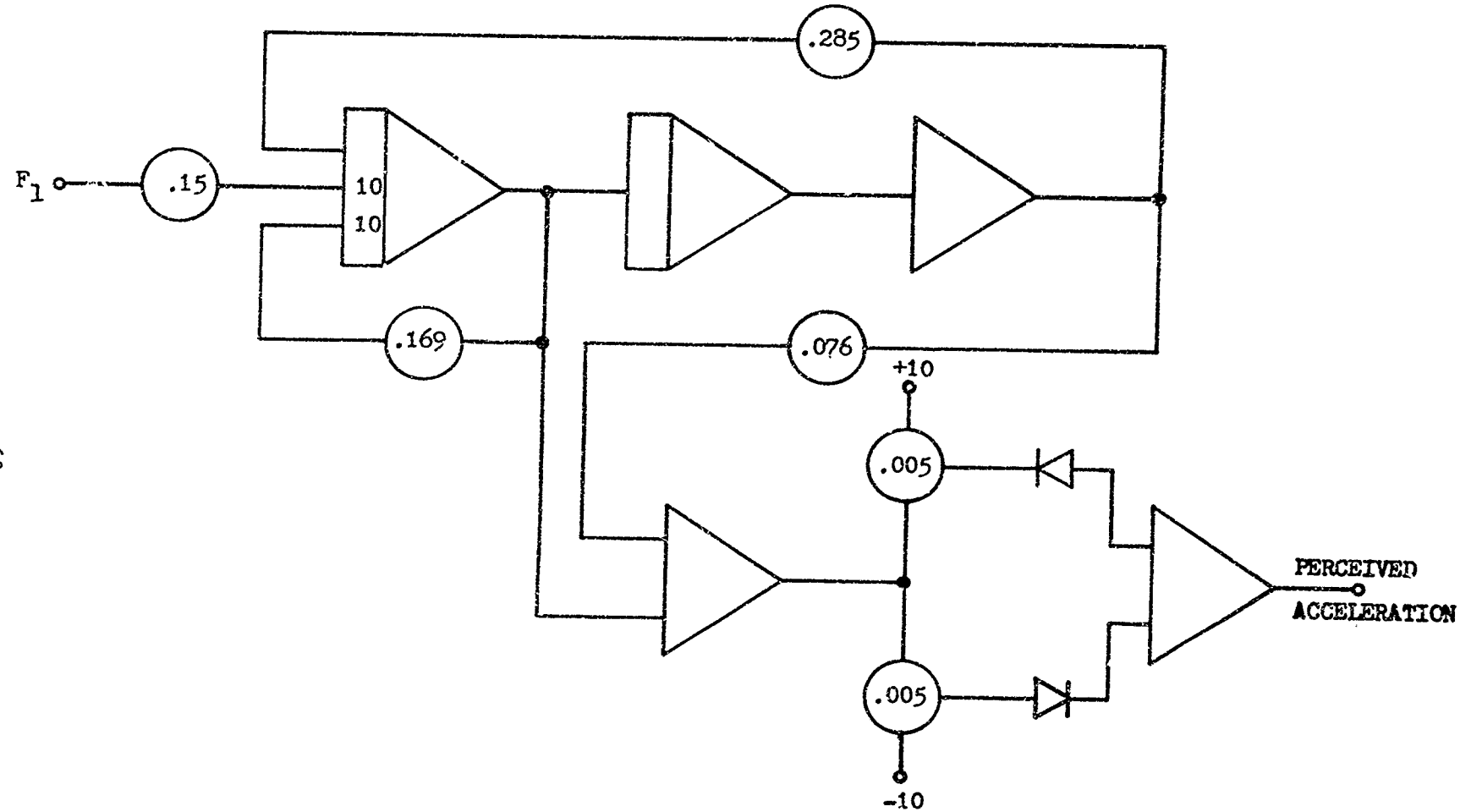


Figure 42. Otolith Model Computer Diagram

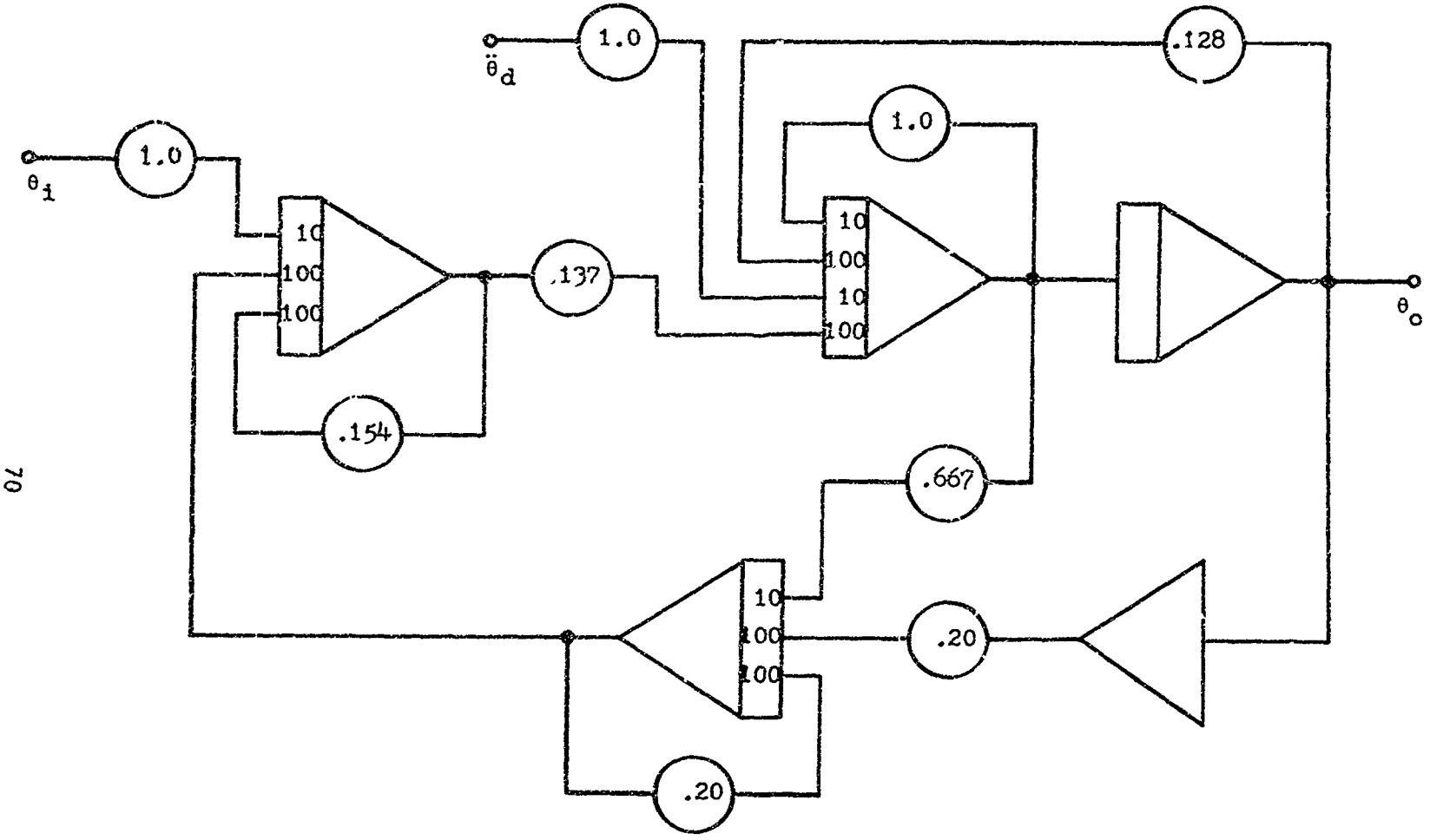


Figure 43. Head/Muscle Model Computer Diagram

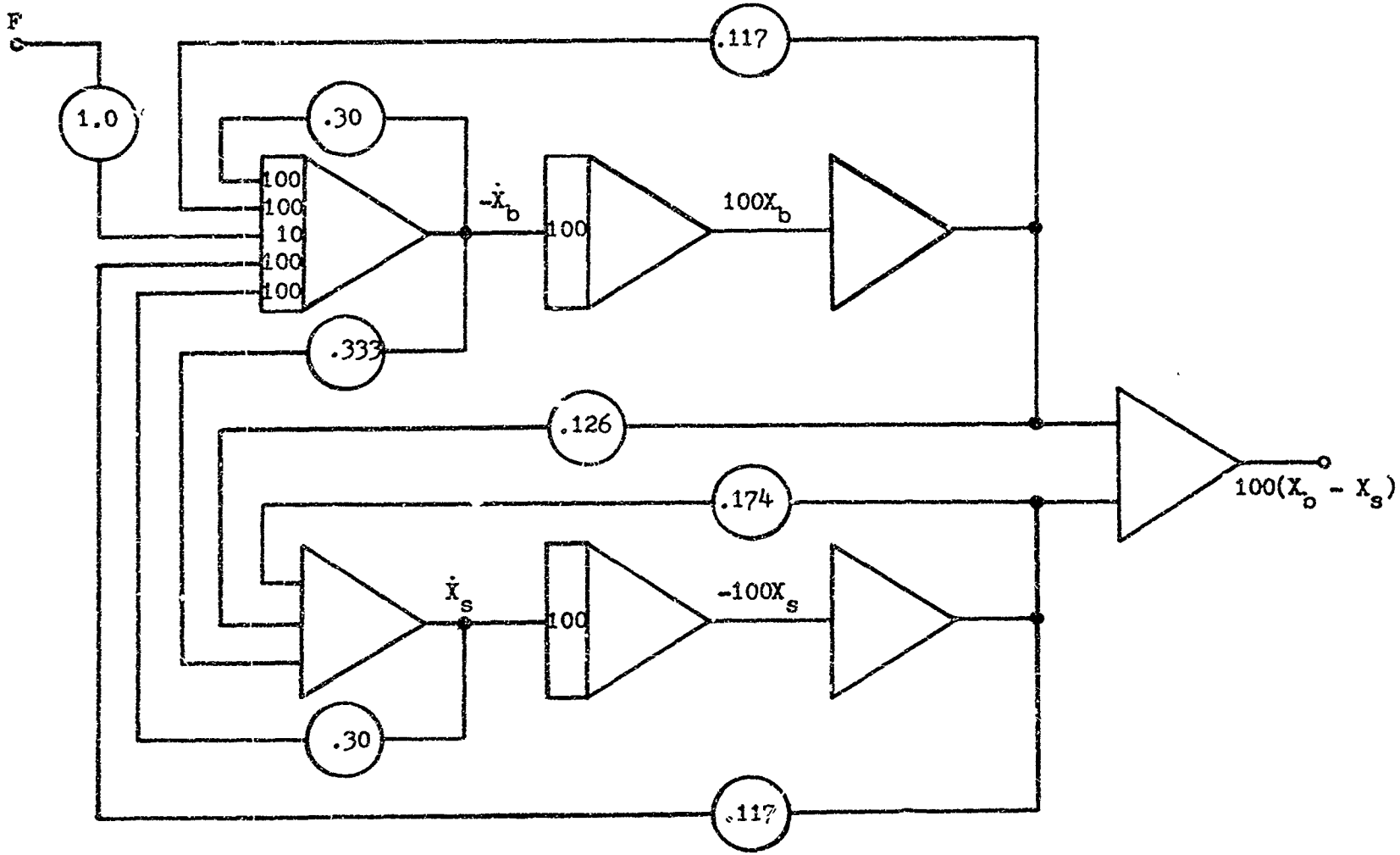


Figure 44. Body/Buttocks/Seat Model Computer Diagram

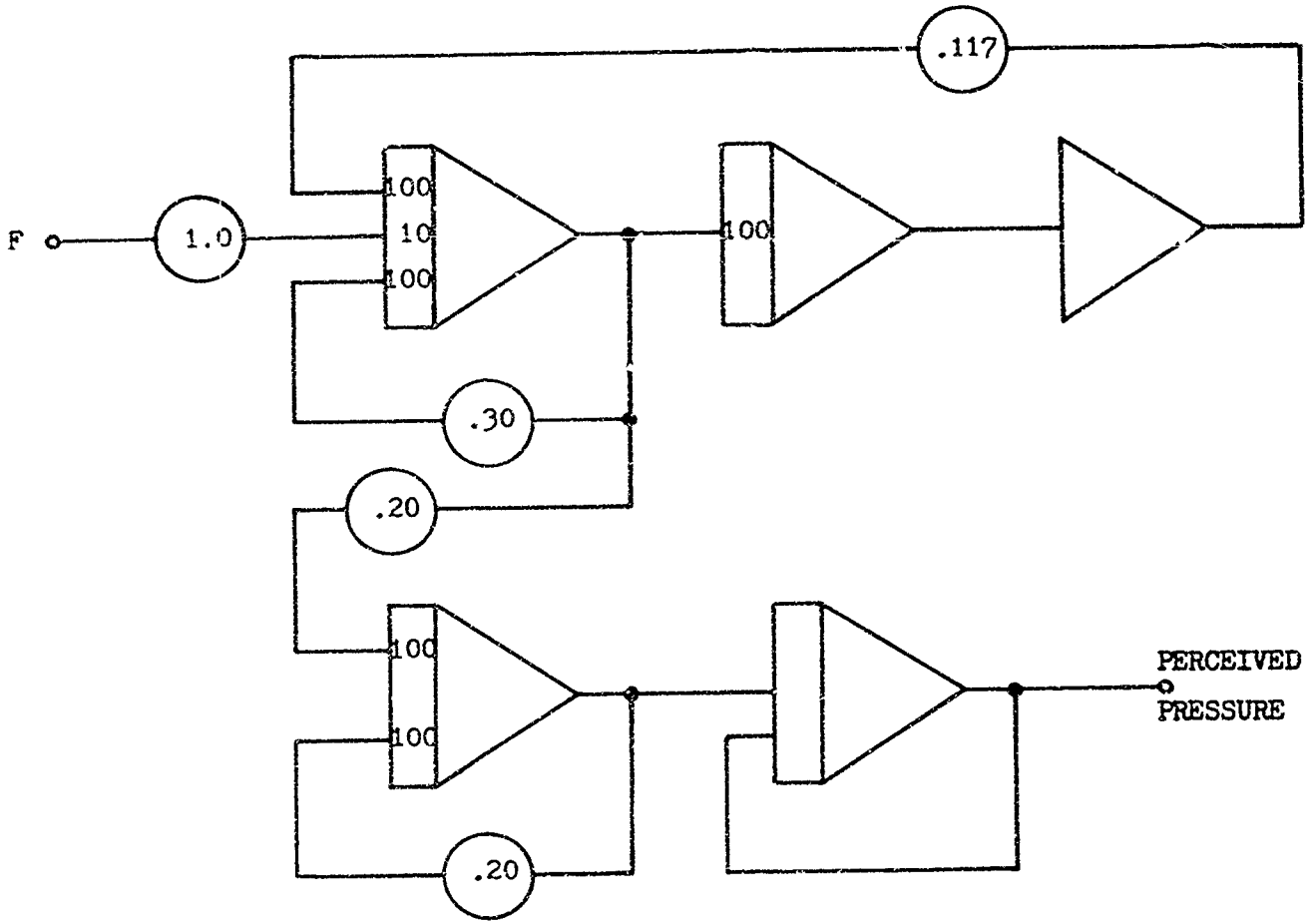


Figure 45. Body Pressure Sensing Model Computer Diagram

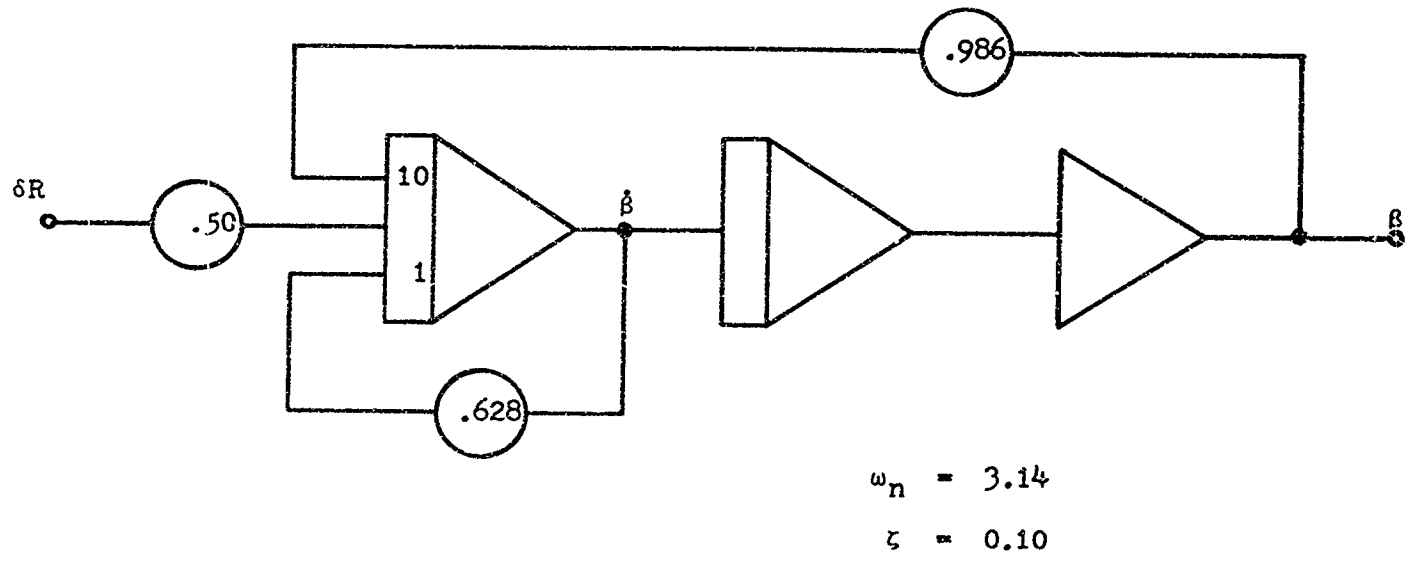


Figure 46. Aircraft Lateral Dynamics Computer Diagram

## APPENDIX B

## HEAD LATERAL MOMENT OF INERTIA CALCULATION

Since data on the moment of inertia of the head about the longitudinal axis could not be found, it was calculated from a crude model formed by two joined right parallelepipeds approximating the head shape. The relative sizes of the two joined right parallelepipeds, the larger representing the head mass above the axis of rotation and the smaller representing the head mass below the axis of rotation, were selected based on shape and relative density. The lower part of the head which includes the cavity of the mouth was considered to have a lower density which was compensated for by reducing its volume. The physical model used is shown in Figure 47.

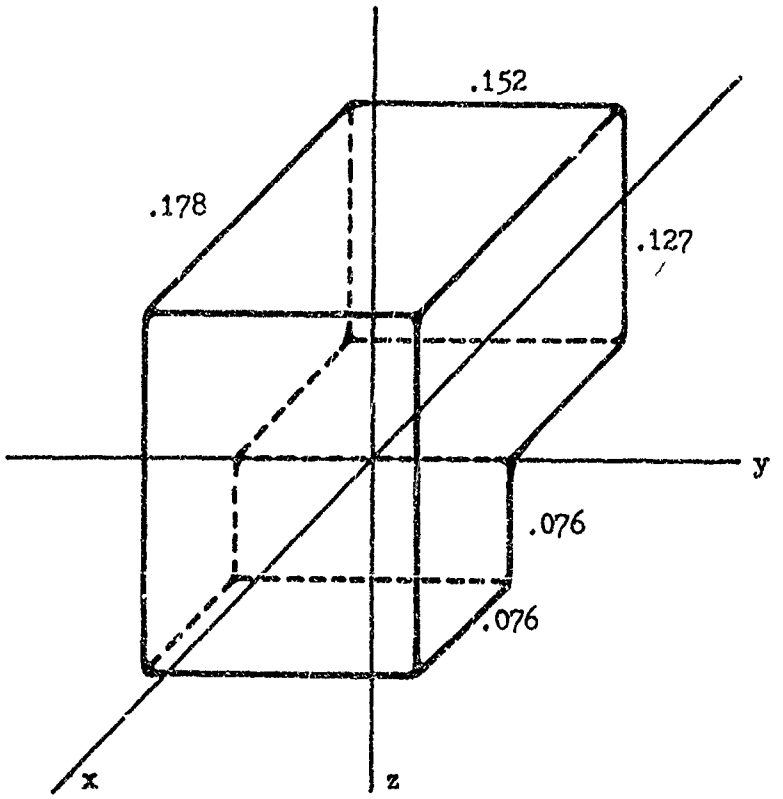


Figure 47. Head Inertia Calculation Model

$$I_x = \rho \int_v (y^2 + z^2)\, dx\, dy\, dz$$

$$I_{x_1} = \rho \int_{-0.076}^{0.102} \int_{-0.076}^{0.076} \int_{0}^{0.127} (y^2 + z^2)\, dx\, dy\, dz$$

$$I_{x_1} = 25.1 \times 10^{-6} \rho \text{ meter}^5$$

$$I_{x_2} = \rho \int_{-0.076}^{0} \int_{-0.076}^{0.076} \int_{-0.076}^{0} (y^2 + z^2)\, dx\, dy\, dz$$

$$I_{x_2} = 3.38 \times 10^{-6} \rho \text{ meter}^5$$

$$I_x = 28.5 \times 10^{-6} \rho \text{ meter}^5$$

Head Volume

$$V_h = 0.00432 \text{ meter}^3$$

Head Mass

$$M_h = 4.6 \text{ kilograms}$$

Density

$$\rho = \frac{M_h}{V_n} = 1.06 \times 10^3 \text{ kilograms/meter}^3$$

Lateral Inertia

$$I_x = 0.0304 \text{ kilogram meter}^2$$

# APPENDIX C
# SUSTAINED FORCE SIMULATION SEAT

Based on the data from Dempsey (References 15 and 16) showing the pressure distribution for the buttocks area and the data taken during this study relating seat force to seat contact area shown in Figure 24, an aircraft simulator seat pan design has been developed. This seat pan, shown in Figure 48, is designed to stimulate in the buttocks primarily (1) the Pacinian corpuscle pressure receptors in the high pressure-loaded areas under the tuberosities and (2) the Meissner corpuscle tactile receptors.

The seat pan would be constructed of 14 individual air-activated compartments of various sizes and shapes. Compartments 8, 9, 12, and 13 would be the same rectangular shape and size. Compartments 5 and 6 would be the same rectangular shape and size but smaller than compartments 8, 9, 12, and 13. Compartments 2 and 3 would be the same shape and size with their upper surface sloping upwards toward the back of the seat. Compartments 7, 10, 11, and 14 would be the same wedged shape and size attached to the top of compartments 8, 9, 12, and 13, respectively. Compartments 1 and 4 would be irregular wedge-shaped compartments attached to the top of compartments 5 and 6, respectively. Located on either side of the center and to the rear of the seat pan directly under the tuberosities would be two high coefficient-of-elasticity pressure blocks. These blocks would be driven bidirectionally in the vertical direction by air-activated pistons.

Under conditions of increased vertical force the following occur: the pressure on the buttocks increases, the pilot sinks in the seat, and the seat/buttocks contact area increases. The opposite occurs for decreased vertical force. To simulate these conditions the seat pan would operate as follows for increased vertical force: (1) the tuberosity pressure blocks would be positioned appropriately to carry

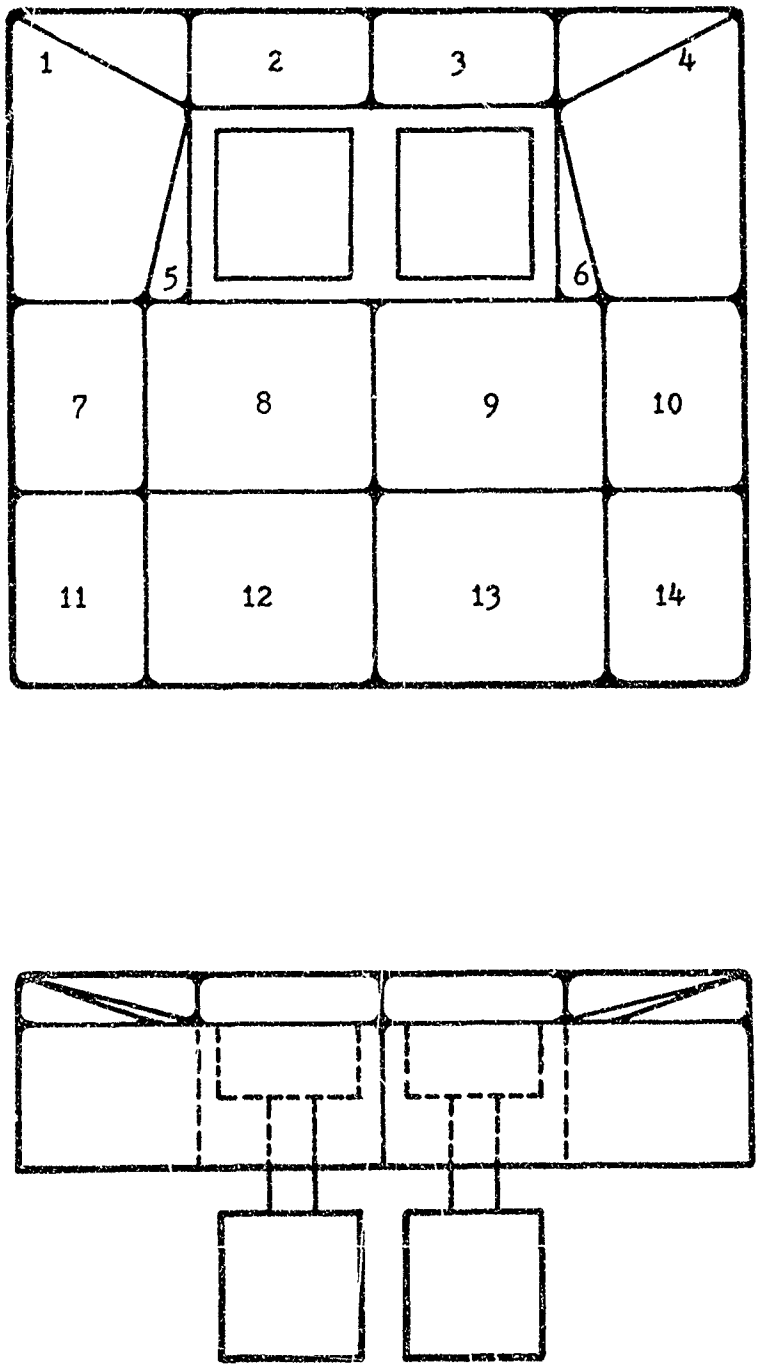


Figure 48. Sustained Force Simulation Seat

a greater part of the total body weight, thereby increasing the pressure under the tuberosity areas; (2) the individual seat compartments would deflate appropriately to lower the pilot in the seat; and (3) the wedge-shaped compartments would be inflated to represent the increase in seat/buttocks contact area. To simulate only vertical forces all of the individual air-activated compartments would not be required; however, to simulate force vectors displaced from vertical, the individual compartments would allow tilting as well as lowering of the seat plane and differential pressure and tactile stimulation of the buttocks areas.

Since the tuberosity areas of the buttocks are the greatest load-carrying and highest pressure areas, with peak pressures about 40 times the average buttocks pressure, air-activated compartments are not considered adequate for this part of the seat. Also, since the pressure sensing mechanism has a relatively rapid response characteristic, the direct variation of applied pressure may be necessary. The pressure blocks would allow the direct application of the required pressure without relying on the inflation or deflation of the surrounding seat compartments. They could be pressure driven with no bias springs so that the applied pressure would be independent of the displacement or elevation of the pressure blocks.

The primary purpose of this seat would be to simulate sustained forces such as those that a pilot experiences during aerobatic flight. The present simulator cockpit moving-base motion systems, which can apply only onset forces, are not capable of simulating sustained forces. Such a seat would most likely find its greatest utility as an augmenter to rather than a replacement for a good moving-base motion system.

The theoretical performance range for the seat can be predicted by considering: (1) the relative areas of the total seat and the

tuberosity blocks, (2) the distribution of the total force (that of the body seat weight), and (3) the resulting pressures on each of the two areas. Consider the following three cases which assume that the force being sensed is directly proportional to the pressure being applied to the tuberosity areas.

| APPLIED FORCE | AREA | FORCE | PRESSURE |
|---|---|---|---|
| | Tuberosity (Total-Tuberosity) | Tuberosity (Total-Tuberosity) | Tuberosity (Total-Tuberosity) |
| g's | $meter^2$ | newtons | $newtons/meter^2$ |
| 1 | 0.0128 | 175 | $13.7 \times 10^3$ |
| | (0.0650) | (375) | $(5.8 \times 10^3)$ |
| 3 | 0.0128 | 525 | $41.1 \times 10^3$ |
| | (0.0650) | (25) | $(0.4 \times 10^3)$ |
| 0.51 | 0.0128 | 90 | $7.1 \times 10^3$ |
| | (0.0650) | (460) | $(7.1 \times 10^3)$ |

The above shows that the theoretical range of operation of the seat is about -0.5 g to +3 g. However, by taking advantage of the apparent rapid adaptation phenomenon of the pressure-sensing mechanism the range of operation could possibly be extended.